AD-A163 809 PARALLEL IMAGE TRANSMISSION THROUGH A SINGLE OPTICAL FIBER(U) ENVIRONMENTAL RESEARCH INST OF MICHIGAN ANN ARBOR A M TAI JAN 86 ERIM-155700-18-F ARO-18283.5-PH 1/1

UNCLASSIFIED DAAG29-81-K-0129 F/G 20/6 NL

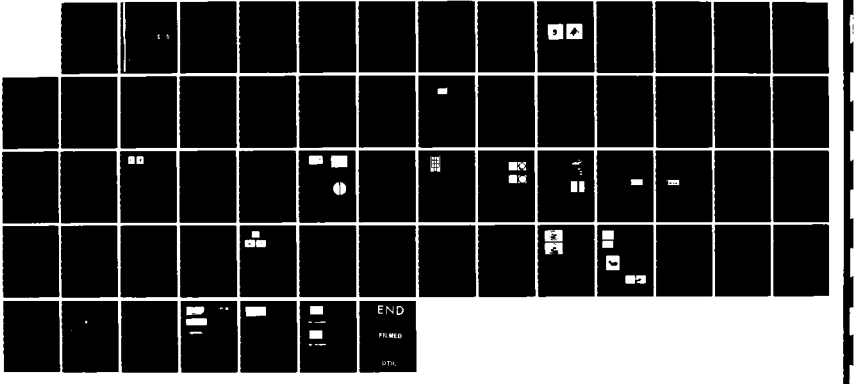

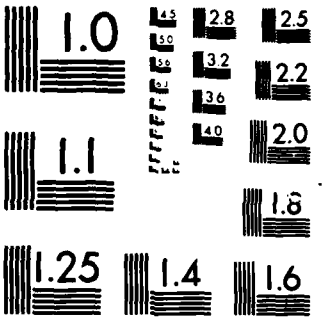

Final Report

PARALLEL IMAGE TRANSMISSION THROUGH A SINGLE OPTICAL FIBER

ANTHONY M. TAI
Infrared and Optics Division

JANUARY 1986

U.S. Army Research Office
P.O. Box 12211
Research Triangle Park, NC 27709
Contract No. DAAG-81-K-0129

ENVIRONMENTAL
RESEARCH INSTITUTE OF MICHIGAN
BOX 8618 • ANN ARBOR • MICHIGAN 48107

UNCLASSIFIED

SECURITY CLASSIFICATION OF THIS PAGE

AD-A 163 809

REPORT DOCUMENTATION PAGE

1a. REPORT SECURITY CLASSIFICATION: UNCLASSIFIED	1b. RESTRICTIVE MARKINGS
2a. SECURITY CLASSIFICATION AUTHORITY	3. DISTRIBUTION/AVAILABILITY OF REPORT
2b. DECLASSIFICATION/DOWNGRADING SCHEDULE	
4. PERFORMING ORGANIZATION REPORT NUMBER(S): 155700-18-F	5. MONITORING ORGANIZATION REPORT NUMBER(S): ARO 18203.5-PH
6a. NAME OF PERFORMING ORGANIZATION: Environmental Research Institute of Michigan; 6b. OFFICE SYMBOL (If applicable)	7a. NAME OF MONITORING ORGANIZATION: U.S. Army Research Office
6c. ADDRESS (City, State and ZIP Code): Infrared and Optics Division, P.O. Box 8618, Ann Arbor, MI 48107	7b. ADDRESS (City, State and ZIP Code): P.O. Box 12211, Research Triangle Park, NC 27709
8a. NAME OF FUNDING/SPONSORING ORGANIZATION; 8b. OFFICE SYMBOL (If applicable)	9. PROCUREMENT INSTRUMENT IDENTIFICATION NUMBER: Contract No. DAAG-81-K-0129
8c. ADDRESS (City, State and ZIP Code)	10. SOURCE OF FUNDING NOS. — PROGRAM ELEMENT NO.; PROJECT NO.; TASK NO.; WORK UNIT NO.
11. TITLE (Include Security Classification): Parallel Image Transmission through a Single Optical Fiber	
12. PERSONAL AUTHOR(S): Anthony M. Tai	
13a. TYPE OF REPORT: Final Report; 13b. TIME COVERED: FROM 6/10/81 TO 11/9/85	14. DATE OF REPORT (Yr., Mo., Day): January 1986; 15. PAGE COUNT: 57
16. SUPPLEMENTARY NOTATION	
17. COSATI CODES — FIELD; GROUP; SUB GR	18. SUBJECT TERMS (Continue on reverse if necessary and identify by block number)

19. ABSTRACT (Continue on reverse if necessary and identify by block number)

New approaches for the transmission of two-dimensional images through a single optical fiber are developed to take better advantages of the bandwidth and the relative immunity to interference offered by optical fibers. Approaches studied include phase-conjunction, matched filtering, axial-angle multiplexing, wavelength multiplexing and various combinations of the approaches. Possible system designs employing these approaches are presented and their relative merits are discussed.

20. DISTRIBUTION/AVAILABILITY OF ABSTRACT: UNCLASSIFIED/UNLIMITED ☐ SAME AS RPT ☐ DTIC USERS ☐	21. ABSTRACT SECURITY CLASSIFICATION
22a. NAME OF RESPONSIBLE INDIVIDUAL	22b. TELEPHONE NUMBER (Include Area Code); 22c. OFFICE SYMBOL

DD FORM 1473, 83 APR — EDITION OF 1 JAN 73 IS OBSOLETE.

SECURITY CLASSIFICATION OF THIS PAGE

PREFACE

The work reported here was performed in the Electro-Optics Department of the Infrared and Optics Division, of the Environmental Research Institute of Michigan (ERIM). This work was sponsored by the U. S. Army Research office under Contract DAAG29-81-K-0129.

The report covered work performed between June 10, 1981 and November 9, 1985. The contract monitor was Dr. B. D. Guenther of the Army Research Office. The principal investigators were Anthony Tai and A. A. Friesem. Major contributors to this effort were Anthony Tai, A. A. Friesem, Jack Cederquist, Y. Silberberg, and Perry Perrault.

CONTENTS

LIST OF FIGURES

1. INTRODUCTION

Optical communication through optical fibers potentially offers higher bandwidth and lower susceptibility to RF interference. Conventional image transmission techniques however, do not fully take advantage of these capabilities. Typically, image transmission is accomplished by first converting a two-dimensional spatial image into a one-dimensional temporal signal with an imaging detector. The temporal signal is then sent through the fiber by modulating the intensity of a light source such as a LED or laser diode. The system basically transmit one pixel at a time; the transmission speed is therefore limited by the scan rate of the imaging detector and the modulation bandwidth of the light source. Moreover, even though the intensity transmittance of an optical fiber is insensitive to external EM fields and radiation, the imaging detector is very susceptible to interference and radiation damage.

The system transmission speed and immunity to interference can be greatly improved if the optical image can be directly transmitted through an optical fiber without the optical-to-electrical signal conversion step. This can be done using a coherent fiber bundle or a Selfoc fiber. The transmission distances that can be practically achieved however, are restricted to a few meters for the fiber bundles and a few centimeters for selfoc fibers. We examined some new approaches for the transmission of two-dimensional images through a single optical fiber. They include the use of phase conjugation, matched filtering, axial-angle multiplexing, wavelength multiplexing and various combinations of the approaches. In this report, the basic approaches are described and possible system implementations are presented. The relative merits of the image transmission techniques are analysed and their usefulness in real world applications are discussed. The main body of the report provides a summary of the results while detailed discussions of the work are given in the appendices. A demonstration system utilizing wavelength-time multiplexing was also

constructed and delivered to the U. S. Army Research Office. The documentation for the demonstration system is provided separately.

2. STATEMENT OF PROBLEM

When a two-dimensional image is projected onto one end of a single strand of multi-mode optical fiber, a scrambled image emerges from the other end. Consider a monochromatic picture field at the input face of the fiber $E(x,y,z=0)$. The input field excites a multiplicity of modes $\phi_m(x,y)$ that propagate through a fiber, each having a complex amplitude of $A_{\ell m}$. The field at the input end of the optical fiber can be written as[1]

$$E(x,y,z=0) = \sum_{\ell,m} A_{\ell m}\phi_{\ell m}(x,y).$$

Each of these guided mode propagates through the fiber at a phase velocity of $\omega/\beta_{\ell m}$. At a distance L at the other end of the fiber we have

$$E(x,y,z=L) = \sum_{\ell m} A_{\ell m}\phi_{\ell m}(x,y)\, e^{i\beta_{\ell m}L}$$

The phases of the different modes are mismatched due to the different phase velocities and the results is a scrambled output. An example is shown in Figure 1.

3. PHASE CONJUGATION

For an input $E(x,y,z=0)$, we obtain at the other end of the fiber $E(x,y,z=L)$. Thus, if we create a conjugate input field of $E^*(x,y,z=L)$, and let it propagates back through an identical fiber, we obtain at the output, $E^*(x,y,z=0)$. That is,[2]

$$\sum_{\ell m} A_{\ell m}\phi_{\ell m} \longrightarrow \sum_{\ell m} A_{\ell m}\phi_{\ell m} e^{i\beta_{\ell m}L}$$

$$\sum_{\ell,m} A^*_{\ell m}\phi^*_{\ell m}\, e^{-i\beta_{\ell m}L} \longrightarrow \sum_{\ell,m} A^*_{\ell m}\phi^*_{\ell m}$$

a b

Figure 1. The Smearing Problem
(a) Image at input face of fiber.
(b) Smeared output.

Since $|E(x,y,z=0)|^2 = |E^*(x,y,z=0)|^2$, we have the desired undistorted image at the output of the fiber. The conjugate field can be generated holographically as illustrated in Figure 2. A separate hologram must be constructed for each image to be transmitted. It is therefore not a very practical approach. Alternatively, a real time conjugate field can be generated with the four-wave mixing technique using a nonlinear optical material such as BSO crystal. One possible arrangement is shown in Figure 3(a). This arrangement however, is also impractical since the input and output images are located at the same side of the optical fiber and the intent is to transmit an image from one end to the other. One solution may be to split the full length of the fiber into two identical halves as illustrated in Figure 3(b). The conjugate field is created after propagating through one half of the total length of the fiber and then launched into the second half of the fiber. If the two halves of the fiber are identical, an undistorted image will emerge from the second fiber. Unfortunately, no two fibers are truely identical due to microscopic differences within the fiber. For a fiber of usable length, the phase velocities in the two halves will exhibit enough mismatches that the output image will remain scrambled.

Since no two fibers are alike, the conjugation filter must be constructed for a specific fiber. We also want the same filter to work with any input image instead of with a specific image as the holographic technique described earlier. This can be achieved by creating an incoherent set of conjugate (matched) filters for each input pixel. Each input pixel will generate an input field at one end of the fiber $E_n(x,y,z=0)$ where upon reaching the other end becomes $E_n(x,y,z=L)$. A composite filter comprising of conjugate filters $E_n^*(x,y,z=L)$ decodes the scrambled field due to each input pixel individually to reconstruct the image. The composite filters can be constructed holographically as shown in Figure 4. The filters are summed together incoherently and it can be described by,

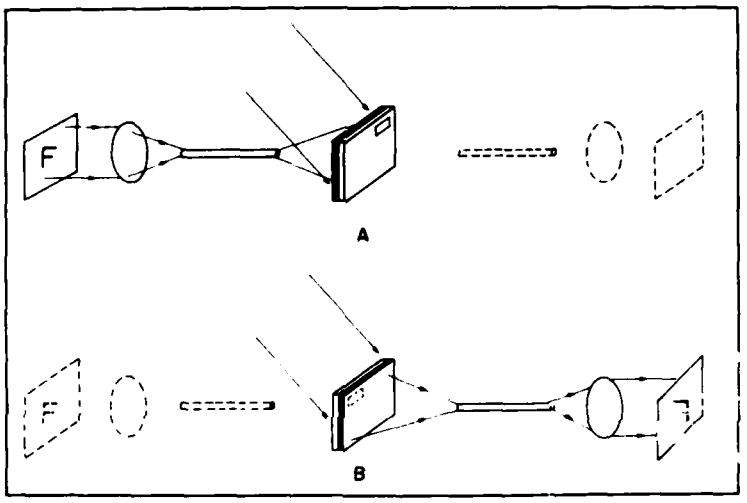

Figure 2. Holographic Phase Conjugation Filter
(a) Recording arrangement.
(b) Readout arrangement.

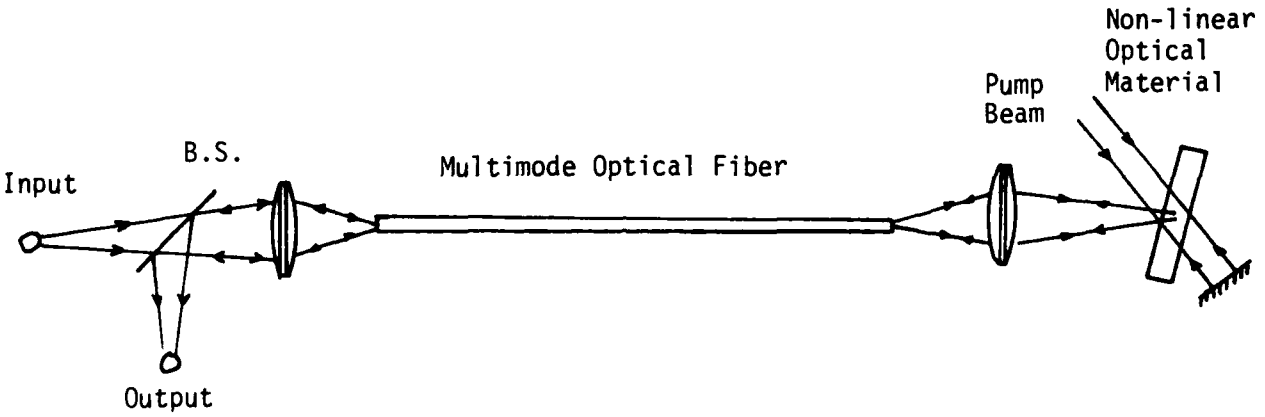

Figure 3(a) Image Transmission using Four-Wave Mixing Technique

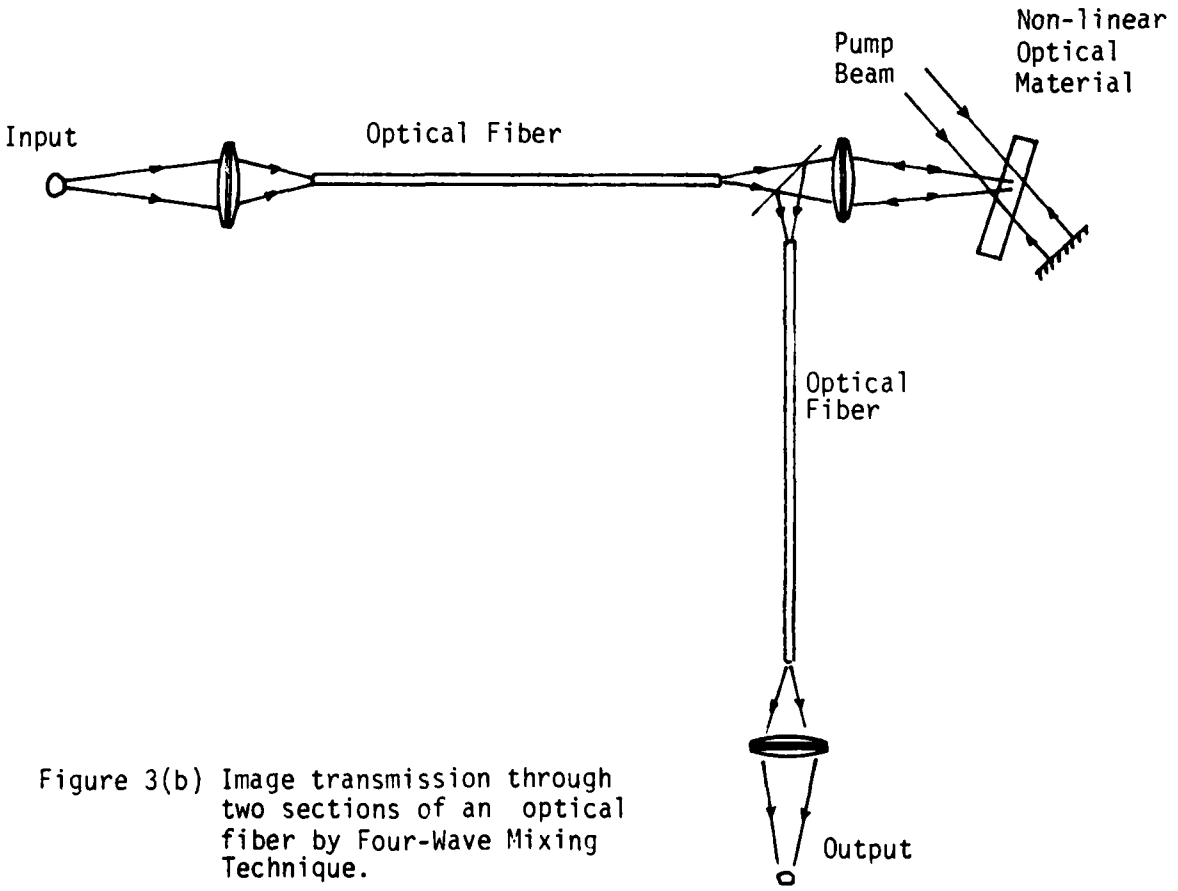

Figure 3(b) Image transmission through two sections of an optical fiber by Four-Wave Mixing Technique.

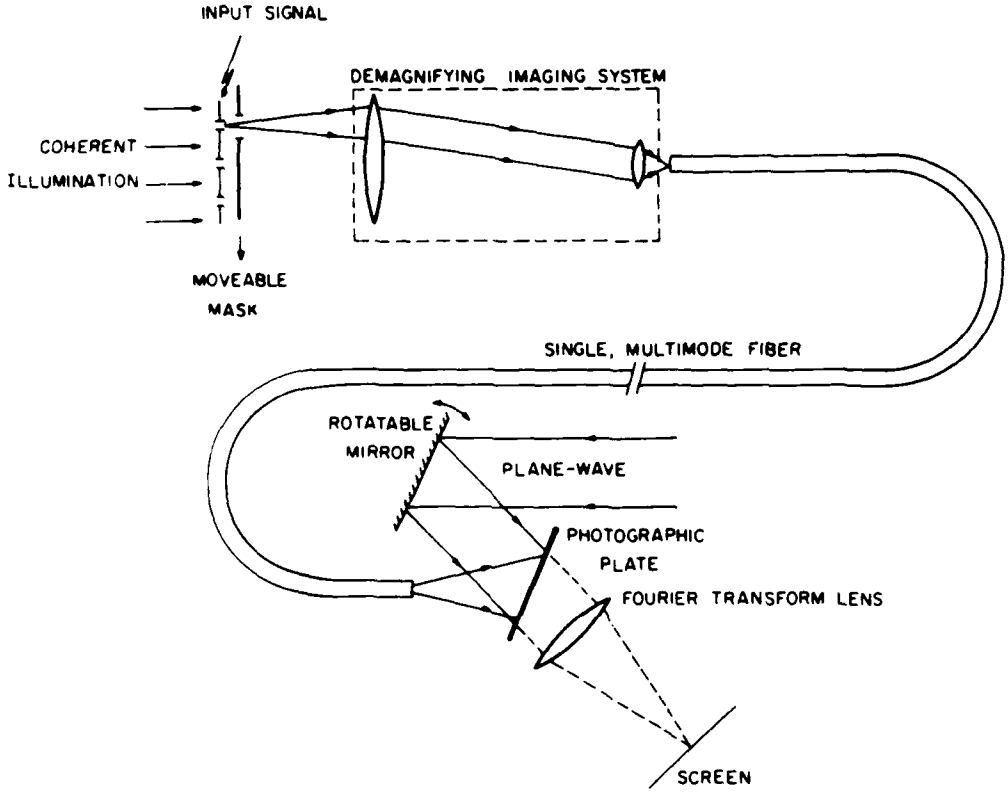

Figure 4. Optical Arrangement for Recording a Holographic Filter and for Transmitting Pictures through a Single Fiber

$$\sum_n |E_n(x,y,z=L) + R_n|^2$$

$$= \sum_n |E_n|^2 + \sum_n |R_n|^2 + \sum_n R_n^* E_n(x,y,z=L)$$

$$+ \sum_n R_n E_n^*(x,y,z=L)$$

where the reference beams R_n are plane waves illuminating the holographic plate at angles determined by the corresponding image pixel. Beside the desired conjugate terms,

$$\sum_n R_n E_n^*(x,y,z=L)$$

we also have many other terms, particularly the bias terms, that are being recorded. Since holographic recording materials possess limited dynamic range, the bias terms severely restrict the number of filters that can be incoherently summed together without the system SNR being reduced to an unacceptable level. Thus, the space-bandwidth product of the image that can be transmitted is limited. There are also other drawbacks. Even though it can be used for the transmission of any image, the composite filter can only be used with the particular fiber with which it is constructed. Moreover, the transmission characteristics of an optical fiber are very sensitive to environmental or mechanical changes. Even minute changes in the fiber temperature or the way it is bent can significantly alter the mode structures and phase velocities of the fiber. The use of phase conjugation for image transmission through a single fiber is therefore not a practical approach except for short lengths of large rigid fibers which are more resistance to changes. Technical details on the use of phase conjugation techniques for image transmission can be found in the paper attached as Appendix A.

4. WAVELENGTH MULTIPLEXING

To utilize more fully the channel capacity of optical fibers, wavelength encoding has been suggested as a means of transmitting images through a single fiber.[2-9] Implementing wavelength encoding-decoding is relatively simple for 1-D images. One may disperse the light emitted from a white-light point source into a line with a grating or a prism, projecting a different wavelength on each pixel of the object to encode the 1-D image. A second grating or prism is used to recombine the dispersed light, which is then coupled into the fiber. At the receiving end of the fiber, the transmitted light is dispersed again by a third grating, recreating the wavelength-encoded input image. Such a system utilizes the light energy efficiently, and there is no additional light loss beside the usual absorption, reflection, and coupling losses.

Extending the wavelength-encoding concept to two dimensions while maintaining high efficiency is a difficult problem. In addition, using wavelength alone to encode 2-D images will severely restrict the space-bandwidth product of the images that can be transmitted. One may compromise by transmitting only one dimension in parallel. The most straightforward implementation is to utilize the 1-D system described earlier and simply translate the input object across the input plane.[6,7] Such an approach is simple but slow, negating the main advantage offered by parallel transmission. Moreover, it is often impossible to translate the object to be imaged. We have developed a much more efficient system approach for the high-speed transmission of 2-D images by wavelength-time multiplexing.[8,9]

To transmit two-dimensional images efficiently and at high speed, a system as illustrated in Figure 5 may be employed. At the transmitting end, a blazed reflection grating is mounted on a scanner which disperses the collimated white light in the x direction while the scanning action scans the dispersed light line across the input object along the y direction. All the elements are placed one focal length apart so that

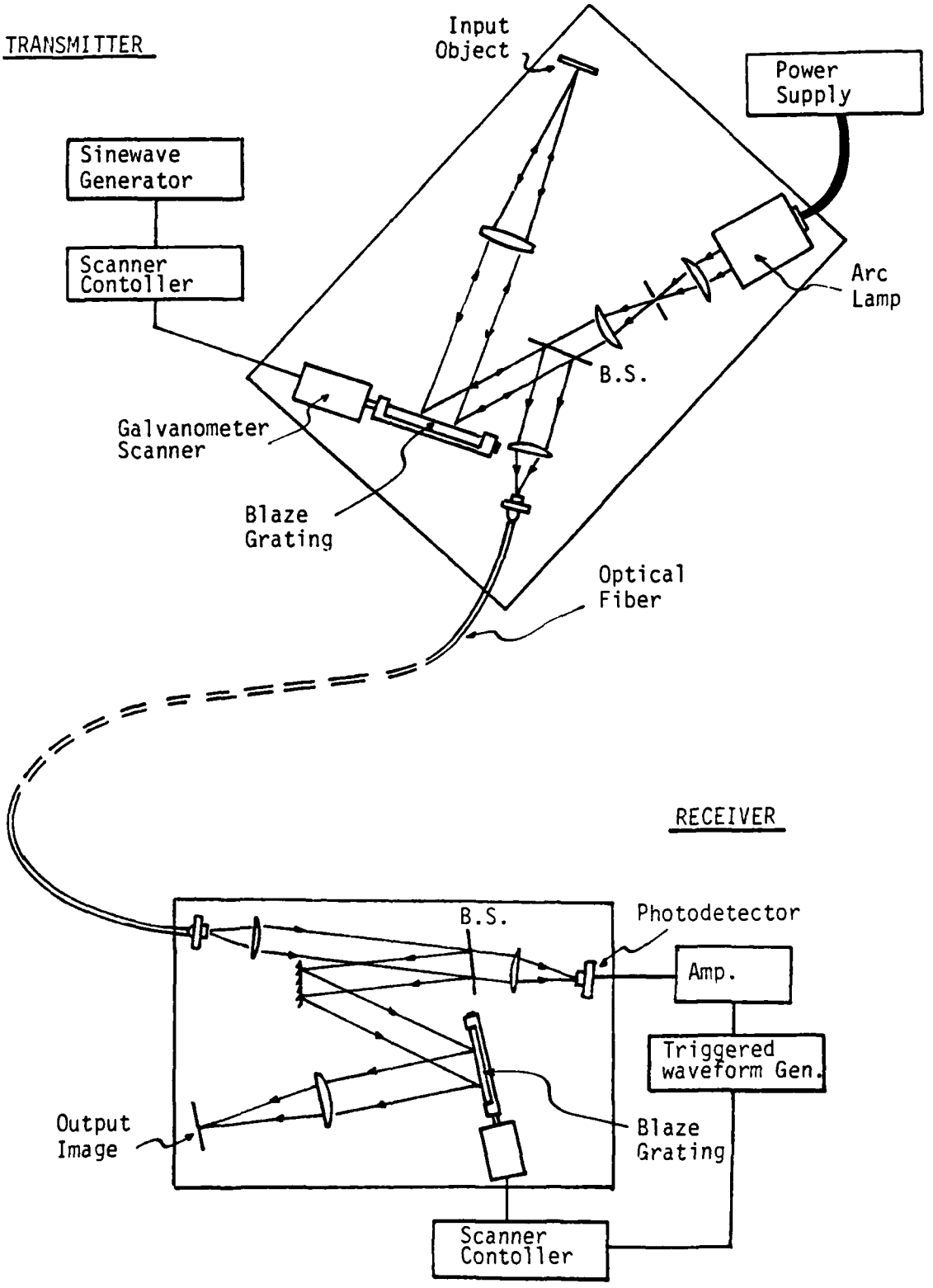

Figure 5 Image Transmission by wavelength-Time Multiplexing.

the reflected light retraces its path and forms a stationary spot (the image of the point source) at the input of the fiber regardless of the position of the scanner. The same grating thus performs the dispersion and scanning of the illuminating beam and the compression of the reflected light back to a single spot to be coupled into the fiber. This optical system can therefore achieve the same high efficiency as the simpler 1-Dimensional system.

To transmit the image of a distant object, it is not possible to synchronize the scanning motors by direct electrical hookup. One possible approach that can be employed to synchronize the scanning motors is to place a small mirror at the object plane. The mirror will reflect strongly, creating a reference that can be used for synchronizing the scanners. The strong return may be used as a trigger for the scanner at the output, or it may be used as a point reference for adjusting the scanner frequency and phase.

A much better approach, however, is to create a self-referencing optical signal that can be used for the synchronization of the scanners. A novel method of generating such a signal is to utilize the second-order diffraction of the encoding grating. By launching the wideband input beam onto the grating at an oblique angle and choosing an appropriate grating geometry, the second-order diffraction can be made to propagate directly back toward the source as illustrated in Figure 5. This creates a color dispersed line that is scanned across the fiber as the grating rotates and produces a single bright spot at the decoded output. The location of the reference spot can be adjusted by changing the geometry of the optics. A color is chosen for the reference light spot so that it appears at the edge of the image field. Since the image is color-encoded, this will allow the reference spot and the target image to be separated using a spectral filter. In our experiment, an interference filter was used as a beam splitter which transmitted the color of the reference spot and reflected all other wavelengths. The reference signal was detected by a photodiode, and the output pulses

were used to trigger a signal generator which in turn was used to drive the scanner. We emphasize that, using this technique, the image transmission and synchronization were performed by optical means with only a single optical fiber connecting the transmitting and receiving ends.

In Appendix C, other possible arrangements are also presented to allow the illuminating light source to be located at the receiving end and to image self-emissive and passively illuminated objects. In addition, design considerations and trade-offs on system parameters such as efficiency, space-bandwidth product and transmittion speed are discussed.

Wavelength multiplexing is probably the most powerful and practical approach for parallel image transmission through a single fiber. If sufficient light power is available, thousands of pixel can be transmitted simultaneously. Even though it is possible to encode a two-dimensional image by wavelengths, the space-bandwidth product of the image that can be transmitted instantaneously is too small to be useful (e.g., 2048 pixels correspond only to a 45x45 image). Restricting the wavelength encoding to a single dimension permit images with large space-bandwidth products to be transmitted. Since one full line of image data consisting of up to thousands of pixels can be transmitted in parallel, the effective data transmission rate is very high. Wavelength multiplexing can also be combined with angle multiplexing to achieve parallel transmission of two-dimensional inputs as will be discussed in the following section.

The encoding of a spatial image by wavelengths has one obvious short coming. It can not be used to transmit images of multi-color objects unless an image conversion is performed using a spatial light modulator as described in Appendix C.

5. AXIAL-ANGLE MULTIPLEXING

The underlying principle for transmitting the angular coordinate by multiplexing is based on the fact that the angle between the propagation direction of a ray of light and the symmetry axis of a step-index fiber is kept unchanged as the ray bounces from the core-clad interface. As proof, consider a ray propagating in the direction $\vec{k} = (k_x, k_y, k_z)$. The axial angle θ is given by $\cos\theta = k_z / \vec{k}$. The magnitude of the vector $\vec{k}$ is obviously unchanged by reflection, and we want to show that the same is true for k_z. Now, the relation between the propagation constant of an emerging beam, $\vec{k}(\text{out})$, and that of an incoming beam $\vec{k}(\text{in})$, due to reflection from a certain plane is given by a reflection matrix [R] as $\vec{k}(\text{out}) = [R]\vec{k}(\text{in})$. Describing the plane by a unit vector $\hat{n} = (n_x, n_y, n_z)$ perpendicular to the plane, it is known [10] that

$$[R] = \begin{bmatrix} 1 - 2n_x^2; & -2n_x n_y; & -2n_x n_z \\ -2n_x n_y; & 1 - 2n_y^2; & -2n_y n_z \\ -2n_x n_z; & -2n_y n_z; & 1 - 2n_z^2 \end{bmatrix}$$

yielding for $n_z = 0$

$$[R]_f = \begin{bmatrix} 1 - 2n_x^2; & -2n_x n_y; & 0 \\ -2n_x n_y; & 1 - 2n_y^2; & 0 \\ 0; & 0; & 1 \end{bmatrix}$$

All the reflections inside the fiber are described by matrices of the type $[R]_f$ for which $n_z = 0$. Clearly, with such matrices, $k_z(\text{out}) = k_z(\text{in})$.

The azimuthal angle, on the other hand, is not preserved. In fact, when a plane wave excites all rays with a given angular (and axial) direction of propagation, the light rays emerging from the fiber will make a conical shell having a uniform density around the cone. As a result of these two effects-axial angle preservation and density uniformity in the azimuthal angle-the light pattern on a screen, some distance away from the output end, is a narrow, uniform ring as shown in Figure 6. A more detailed discussion of the far field output pattern due to a oblique plane-wave excitated is given in Appendix A.

To efficiently decode the output, each cones of light emerging from the fiber must be collected and compressed back to a single image pixel at the appropriate position. This can be achieved using a computer generated hologram (CGH) that transforms rings to points with the radius of the ring corresponding to the position of the point along a line as illustrated in Figure 7. The design and fabrication of such a CGH is described in Appendix D.

6. ANGLE WAVELENGTH MULTIPLEXING

Since the output is circularly symmetric along the optical axis of the fiber, axial-angle multiplexing can only be used to transmit one-dimensional images. Angle-time multiplexing can be used to transmit two-dimensional images employing a scanning techniques similar to that presented for wavelength-time multiplexing. Alternatively, angle multiplexing can be combined with wavelength multiplexing to achieve instantaneous parallel transmission of two-dimensional images. The output decoding can be performed with the same rings-to-line hologram described earlier but with a large spatial carrier offset added. Devices used to write CGH is limited in resolution and the carrier spatial frequency that can be generated is therefore quite small. To decode a wavelength multiplexed signal requires a highly dispersive element. A rings-to-line hologram with a large spatial carrier can be obtained by copying the CGH holographically onto a second holographic

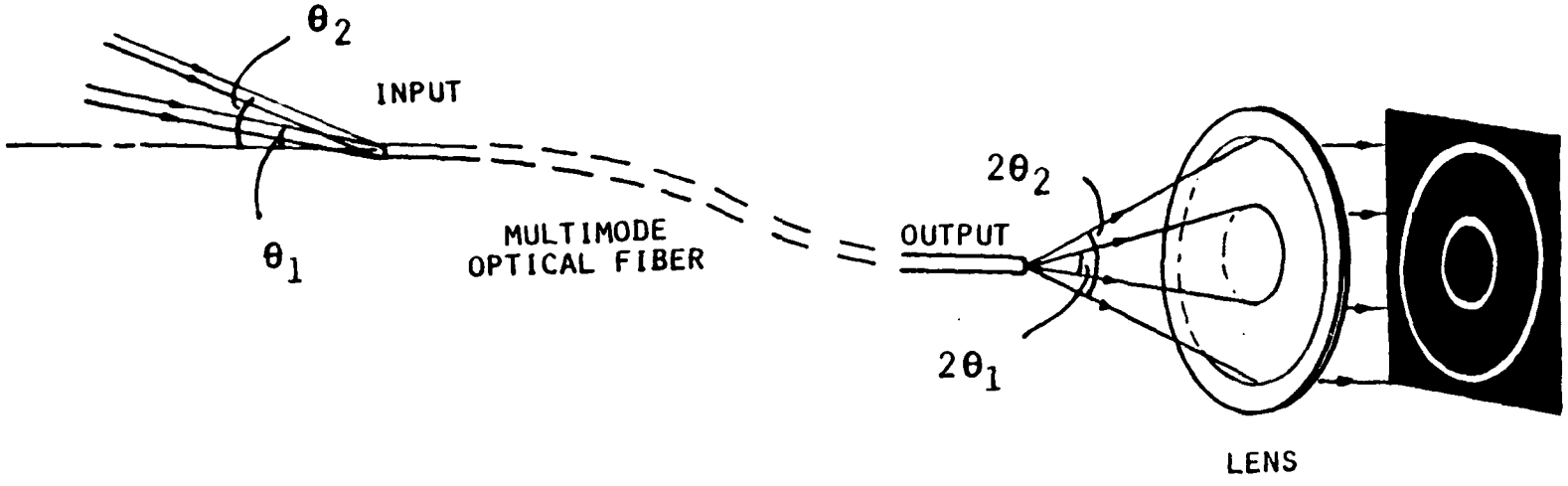

Figure 6. Axial-Angle Multiplexing.

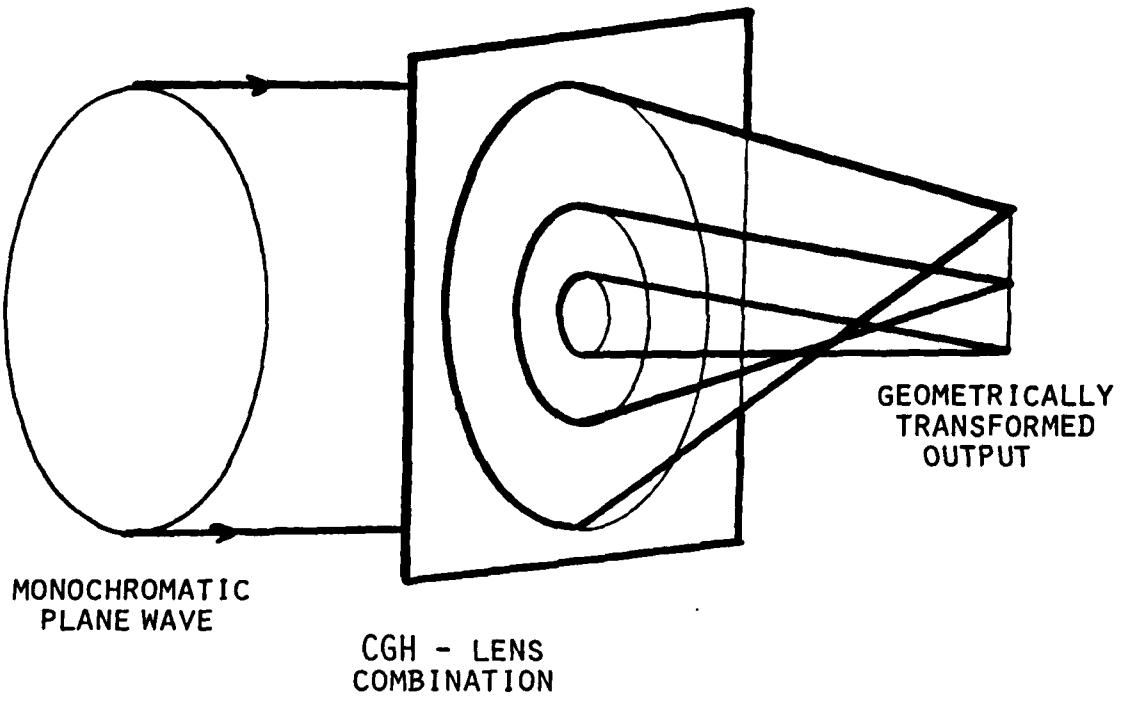

Figure 7. Computer Generated Hologram that Transforms Rings to Points along a Line with the Radius of the Ring corresponding to the Position of the Point along the Line.

plate with a large reference beam angle as shown in Figure 8. A possible communication system utilizing angle-wavelength multiplexing is given in Figure 9. The input is multiplexed by axial angle in the x direction and by wavelength in the y direction. The hologram at the output takes light from rings of different radii and forms a line along the x direction while the spatial carrier disperses the light in the y direction. As explained in Appendix A, the number of discrete pixels that can be transmitted via angle multiplexing decreases rapidly with transmission length. Except for very short data links (a few meters), the small number of pixels that can be encoded by axial angle is too limited for the transmission of images. However, angle-multiplexing can be very useful for multiplexing conventional optical communication channels. Ten pixels along one dimension may be useless for image encoding but a ten folds increase in communication channel is a substantial improvement. Wavelength multiplexing is commonly used to transmit multiple parallel channels through a single fiber. However, the range of emission wavelengths that can be obtained from laser diodes is limited and the emission wavelength is hard to control. The number of wavelength-multiplexed channels is therefore restricted. The combination of angle and wavelength multiplexing makes it possible to increase the number of multiplexed channels by many folds without having to pack the channels closer together in wavelengths.

7. Summary

We have examined several new approaches for image transmission through a single optical fiber including phase conjugation, wavelength and axial-angle multiplexing. Their performance characteristics and viabilities are analysed and specific system implementations of the approaches are presented.

Phase conjugation does not require any encoding of the input and it is therefore the desired approach for applications where there are no room for encoding optics (i.e. observing events in a small inaccessable

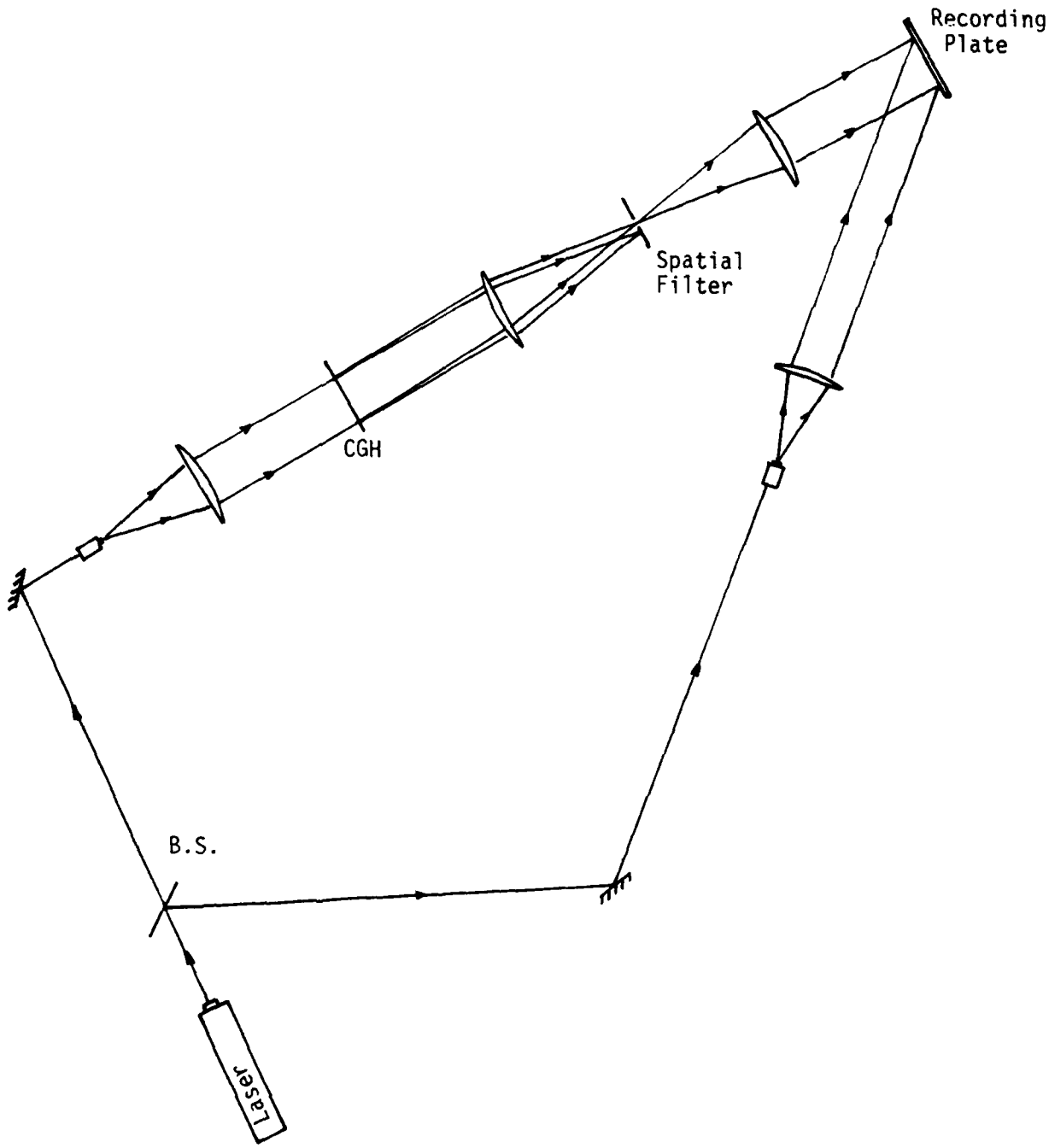

Figure 8 Copying of a Computer-Generated Hologram to generate a Computer-Originated-Hologram with a Large Off-set Angle.

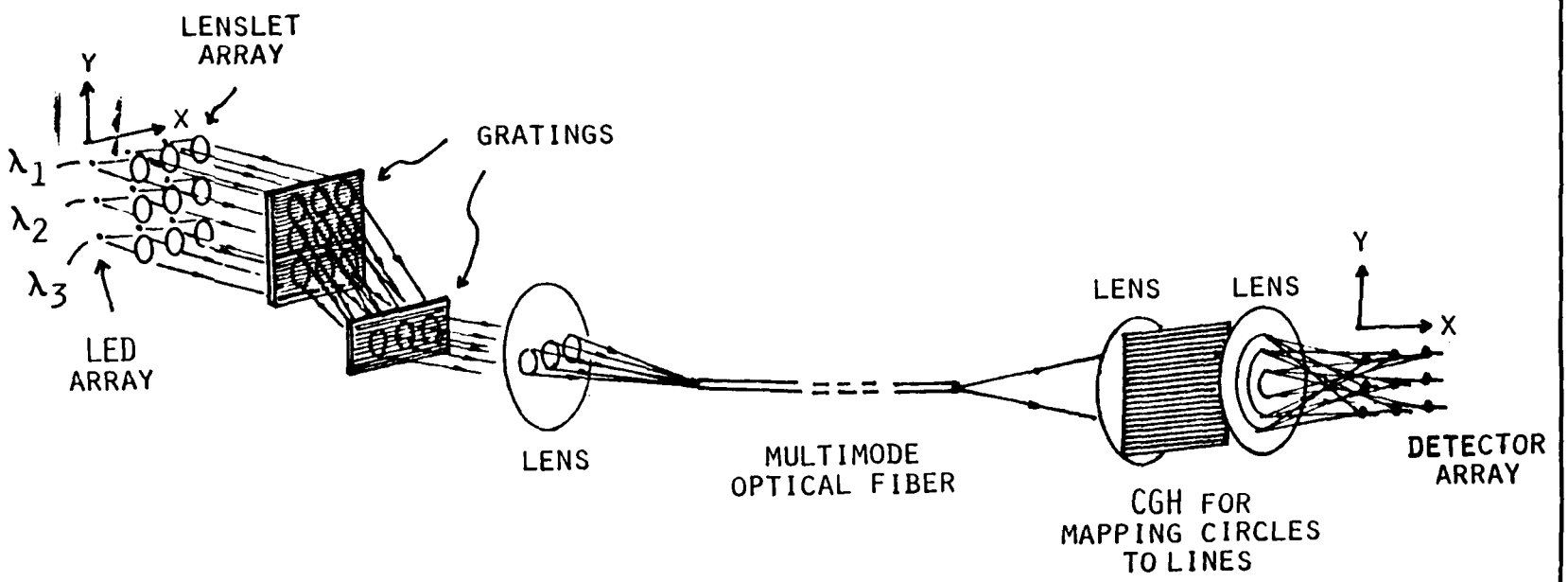

Figure 9. An Optical Communcation System Employing Angle-Wavelength Multiplexing

space). However, the transmission length that can be used is very limited and only large rigid fibers can be used. Angle-multiplexing suffers similar drawbacks but to a much lesser extent. The number of pixels that can be transmitted via axial-angle multiplexing decreases with transmission length and the space-bandwidth product may be too small to be useful for image transmission. However, the approach may be useful in conventional optical communication systems where several folds increase in the number of parallel optical channels would represent a significant improvement. Wavelength multiplexing remains the most powerful and practical approach for parallel transmission of image data. We have presented an efficient system implementation employing wavelength-time multiplexing for the transmission of two-dimensional images with large space-bandwidth products through a single optical fiber. The system performance is quite insensitive to the transmission length except for the normal attenuation and power budget considerations. The main draw back of this approach is that images of multi-color objects cannot be transmitted without a signal conversion step.

The proposed techniques for image transmission through a single optical fiber are expected to be useful in the following applications: 1) Real time remote observation of rapidly changing or short-lived events 2) Remote observation in a hostile environment where an active device such as an imaging detector cannot survive 3) Transmission of images with large space-bandwidth product at high speed.

REFERENCES

1) A. Grover, C.P. Lee and A. Yariv, J. Opt. Soc. Am. Vol.66, p.306 (1976)

2) A. Friesem, U. Levy and Y. Silberberg, Proc. IEEE, Vol. 72, p.208 (1983)

3) A.A. Friesem and U. Levy, Opt. Letteres, Vol.2, p.133, (1978)

4) J.D. Armitage et al. Jpn. J. Appl. Phys., Vol.4, p.273 (1965)

5) H.O. Bartelt, Opt. Comm. Vol.27, p.365 (1978)

6) B. Adams and S. Case, Appl. Opt. Vol.22, p.2026 (1983)

7) D.E. Husley and S. Case, Appl. Opt. Vol.22, p.2029 (1983)

8) A. Tai and A. Friesem, Opt. Letters, Vol.8, p.57 (1983)

9) A. Tai, Appl. Opt., Vol.22, p.3832 (1983)

10) W. Bronwer, Matrix Mathod in Optical Instrument Design , New York, W.A. Benjamin (1964)

Appendix A

Parallel Transmission of Images Through Single Optical Fibers

Published in Proceedings of the IEEE, Vol.71, NO.2, Feb. 1983

Parallel Transmission of Images Through Single Optical Fibers

A. A. FRIESEM, SENIOR MEMBER, IEEE, URI LEVY, MEMBER, IEEE, AND YARON SILBERBERG

Abstract—The characteristics and limits of parallel transmission of two-dimensional imagery through single optical fibers are reviewed, and methods for overcoming the inherent smearing that occurs at the output are discussed. These solutions include: a) control of the fiber's refractive index profile; b) incorporation of complex filters; and c) encoding the information at the input and decoding the output after transmission.

I. INTRODUCTION

WIDESPREAD INTEREST in fiber optics was probably first stimulated by K. C. Kao and G. A. Hockham in 1966 [1], who predicted that in optical fibers drawn from pure fused silica glass losses could be less than 20 dB/km. This prediction triggered an explosive growth in the high-quality fibers and related electrooptical components. Although the main emphasis has been on incorporating these two elements for communication systems, other optical fiber applications have flourished as well. One such application is parallel image transmissions through fibers.

The most common method for parallel imaging by fibers was proposed over fifty years ago [2]. It involves an ordered bundle of fibers in which each individual fiber transmits only one resolution element of the image from one end to the other. Although simple and reliable, this method could not be practically implemented until the technology for fabricating low-loss ordered bundles of many fibers was developed by N. S. Kapany and H. H. Hopkins [3], and more recently by W. P. Siegmund [4]. At present, high-quality "fiberscopes," as these bundles are sometimes called, are routinely exploited for medical diagnosis and other imaging applications. However, the production of such bundles containing a large number of properly arranged fibers is relatively difficult, and they are limited to lengths of less than 5 m.

A potentially more promising approach for parallel image transmission through long fibers is to exploit the large information carrying capacity of single multimode fibers. Indeed, it is reasonable to assume that the number of resolution elements or channels that can be simultaneously transmitted is proportional to the number of modes that are supported by the fiber guide. Unfortunately, when an image is transmitted directly by a single optical fiber, the output is invariably smeared, as illustrated in Fig. 1. This smearing occurs because there is no one-to-one correspondence between input and output points as is required for imaging. For example, two rays emanating from a single point of light at the input face can propagate through the fiber to reach two different points at the output face. Alternatively, inverting the roles of input and output faces (analogous to time reversal), it is also possible that rays from two different input points may coincide to form one output point. Some sophisticated optical fibers having either a graded or more complex refractive index pro-

Manuscript received July 1, 1982; revised October 21, 1982. This work was supported in part under Grants from the United States Army Research Office and the Israel National Council for Research and Development. Part of this work was performed under the auspices of the Environmental Research Institute of Michigan.

A. A. Friesem and Y. Silberberg are with the Weizmann Institute of Science, Rehovot, Israel.

U. Levy is with Bell Laboratories, Murray Hill, NJ 07974.

0018-9219/83/0200-0208$01.00 © 1983 IEEE

(a) (b)

Fig. 1. The smearing problem. (a) Image at input face of fiber. (b) smeared output.

file do have imaging capabilities, but, as we shall subsequently show, their imaging lengths are rather limited.

In this paper we explore a number of techniques for overcoming the smearing problem, so as to allow direct image transfer through a single fiber. These will include: a) control of the fiber's geometry and refractive index profile; b) incorporation of complex filters to compensate for the smearing; and c) encoding the information at the input by means of either angular or wavelength or time multiplexing, or some combination of these, and decoding the output after transmission.

II. Basic Relations

In this section, we shall consider the imaging properties of optical fibers in terms of the modes that propagate through them. We begin with Maxwell's wave equations, which can be simplified for cylindrically symmetric waveguides by assuming that all six components of the field have the same distance and time dependence of the form $\exp[i(\beta z - wt)]$; where z is a coordinate parallel to the axis of symmetry, w is the angular frequency of the sinusoidally varying fields, and β is the propagation constant. This simplification leads to Helmholtz equation of the form [5]

$$\nabla_t^2 E_z + [k_0^2 n^2 - \beta^2] E_z = 0$$
$$\nabla_t^2 H_z + [k_0^2 n^2 - \beta^2] H_z = 0 \qquad (1)$$

where ∇_t^2 is a Laplacian in the transverse coordinates, E_z and H_z are the longitudinal components of the electric and magnetic fields, respectively, k_0 is the free space propagation constant, and n is the refractive index which is assumed constant.

For the special case of a circular step-index fiber, (1), given in cylindrical coordinates, becomes the well-known differential equations for Bessel functions, and the propagation constants are determined by the continuity conditions imposed on the fields at the core-clad boundary. The solution associated with a given value of the propagation constant is usually referred to as a normal mode. There are a finite number of guided modes associated with a finite, discrete set of propagation constants in the range $k_0 n_2 \leqslant \beta$ (guided modes) $\leqslant k_0 n_1$, where n_1 and n_2 are the refractive indices of the core and clad, respectively. There is also a continuum of radiative modes with propagation constants in the range $0 \leqslant \beta$ (radiating modes) $\leqslant k_0 n_2$.

If the dielectric constant of the waveguide varies slowly compared to the wavelength, the solutions to (1) represent good approximations to the solutions of the more complete equation which contains a term that involves the gradient of the dielectric constant. The assumption of small refractive index variations is usually made in the case of a fiber with parabolic refractive index cross section, and each component of the field has to satisfy the Helmholtz equation. Again, a finite set of functions (guided modes) provide a solution to the field equation, subject to the condition that they vanish far away from the center. The normal modes are orthogonal to each other and form a complete set. The completeness is very important in the present context because it means that any input field can be expressed as a linear combination of the normal modes.

Consider a monochromatic picture field at the input face of the fiber $E(x, y, z = 0)$. This field excites a multiplicity of modes that can propagate through the fiber, $\phi_{lm}(x, y)$, each having a strength and phase given by the complex coefficient A_{lm}

$$E(x, y, z = 0) = \sum_{l,m} A_{lm} \phi_{lm}(x, y). \qquad (2)$$

Of course, a continuum of radiative modes are also excited, but we assume that they carry only a small fraction of the total energy in the picture field and, therefore, neglect them in (2). Each of the guided modes propagates with a certain phase velocity ω/β_{lm}, and at a distance L from the fiber the field becomes

$$E(x, y, z = L) = \sum_{l,m} A_{lm} \phi_{lm}(x, y)\, e^{i\beta_{lm} L} \qquad (3)$$

Equation (3) provides an explicit formulation of the imaging problem, it is the difference in phase velocity of the guided modes that causes the smear of the picture after propagating a certain distance through the fiber.

In 1975, Gover, Lee, and Yariv [6] explored the theoretical aspects of the problem and suggested a straightforward solution. First, perform a "segregation transformation" on the field at the output so that each mode is spatially separated from all others. Next, introduce a phase compensation in which each (l, m) mode is multiplied by a phase factor $\exp[-i\beta_{lm} L]$, and finally perform the inverse segregation transformation to obtain a replica of the input field. They correctly stated that their solution relies on the existence of the segregation transformation. Unfortunately, such segregation is extremely difficult, if at all possible, with conventional waveguides. Moreover, even if separation of the modes were possible, it is unlikely that a compensation filter, which would be designed for an ideal fiber, could perform adequately for real (nonideal) fibers.

As a different solution to the smearing problem, we could conceive that a set of propagation constants $\{\beta_{lm}\}$ exists such that, at a certain distance L_I, the relation

$$\beta_{lm} L_I = \text{integer} \cdot 2\pi + \text{constant} \qquad (4)$$

is satisfied. Then, at this distance, the phase factors $\exp[i\beta_{lm} L_I]$ in (3) do not differ from each other yielding an output which is essentially a replica of the input picture field. The simplest distribution of the propagation constants that fulfills (4) is such that they are equally spaced. Suppose, for example, that the propagation constants depend on only one (integer) quantum number q and are spaced according to $\beta_q = \beta_0 - q\alpha$, then at distances $L_s = s(2\pi/\alpha)$, $s = 1, 2, \cdots$, (4) is satisfied; namely, images are obtained periodically along the fiber waveguide with a period of $2\pi/\alpha$. In the following section, we shall consider optical guides that have the desired distribution of propagation constants.

III. Fibers with Controlled Geometry and Index Profile

There are two classes of fiber waveguides in which modes propagate with constants that are approximately equally spaced. The first is a class of polygonal waveguides and the second is a class of graded index fibers. Traditionally, the imaging properties of the two classes are known as self-imaging and self-focusing, respectively.

A. Self-Imaging

The propagation constants of TE modes in a metallic slab waveguide are given as [7]

$$\beta_m = k_0 \left[1 - \frac{1}{k_0^2}\left(\frac{m\pi}{d}\right)^2\right]^{1/2} \tag{5}$$

where d is the width of the slab. In the paraxial approximation (i.e., small m) (5) simplifies to $\beta_m \sim k_0 - m^2\alpha$ with $\alpha = (1/2\,k_0)\cdot(\pi/d)^2$; hence, the distance between successive image planes is $8\,d^2/\lambda$. When inverted images are included, the distance between successive image planes decreases to $4\,d^2/\lambda$. An alternative approach for analyzing properties of slab waveguides is to consider the walls of the guides as mirrors which reflect the input to form a periodic lattice of virtual images having a period of $2d$. Such periodic structures have self-imaging properties as was first observed by H. E. Talbot [8] and analyzed by Rayleigh [9] and later on by others [10]-[12]. Clearly, periodic structures are formed also by waveguides which have a triangular, rectangular, hexagonal, and other polygonal cross sections [11], [13]. Even a circular waveguide can form a self-image of a point source located on-axis [14].

Unlike metallic waveguides, the beam of light that bounces off the core-clad boundary in dielectric waveguides suffers a phase shift which, in addition to dependence on the angle of incidence, also depends on polarization. Hence, the expression for the propagation constants of the modes in a slab dielectric waveguide are more complicated than the relatively simple expression given in (5). Nevertheless, dielectric waveguides of polygonal cross section do possess the self-imaging property [15], but imaging is confined to short distances, typically a few centimeters, and is not applicable to the most common round fibers. The more sophisticated graded-index fibers, on the other hand, have self-focusing properties and are more suitable for relaying images.

B. Self-Focusing

The values of the propagation constants that characterize an optical waveguide are primarily determined by the cross-sectional index of refraction profile of the guide. This profile can be so chosen, at least theoretically, that the propagation constants are equally spaced, thereby leading to a guide having imaging properties. We refer to these properties as self-focusing.

For a two-dimensional (slab) waveguide, the index profile, $n(x)$, must have the following form:

$$n^2(x) = n_0^2 \operatorname{sech}^2(\alpha x). \tag{6}$$

For this profile the propagation constants are equally spaced [16] according to

$$\beta_m = [(\alpha/2)^2 + k_0^2 n_0^2]^{1/2} - \alpha(m + \tfrac{1}{2}). \tag{7}$$

An important difference between self-imaging and self-focusing becomes evident by juxtaposing (5) and (7). In (5), the spacing between the propagation constants depends heavily on the wavelength of light, whereas in (7) the dependence of the spacing, α, on wavelength is negligible. Consequently, self-imaging occurs in different planes for different wavelengths, while for self-focusing the picture fields at all wavelengths are essentially focused at the same plane. Thus self-imaging applies to monochromatic fields only, whereas self-focusing applies to polychromatic fields.

The fact that the hyperbolic secant is the ideal profile for image transmission in a two-dimensional waveguide was first discovered by A. L. Mikaelyan in 1951 [17], and, later on, by several other scientists through quite different approaches such as Abel's integral equation [18], ray optics (Eikonal Equation) [19], Green's function [16], and group velocity and W. K. B. approximation [20].

It should be noted that the refractive index distribution, given in (6), vanishes as x approaches infinity. However, practical waveguides do not have infinite width and the refractive index is greater than one. In fact, the profile is truncated at some distance, thereby shifting the propagation constants (mainly higher orders) so that the waveguide ceases to be ideal. In this connection, it is worthwhile to mention another refractive index profile which also yields self-focusing. This profile is analogous to a quantum mechanical potential known as Morse potential [21]

$$n^2(x) = n_0^2[2\exp(-\alpha x) - \exp(-2\alpha x)]. \tag{8}$$

This profile (which obviously is impractical) yields the following family of propagation constants:

$$\beta_m = k_0 n_0 - \alpha(m + 1/2) \tag{9}$$

as required for perfect self-focusing. Thus, at least theoretically, slab waveguides may transmit images perfectly, provided they have the appropriate refractive index profile. However, such waveguides are not attractive because they are relatively difficult to fabricate and their mechanical properties are inferior, and mainly because they transmit only one-dimensional light distributions.

Potentially, three-dimensional, round fibers are much more promising, but, unfortunately, no ideal profile has thus far been found. Indeed, as we will show, it is unlikely that an ideal profile for long transmission length exists.

It is a well-known fact [22] that a parabolic index fiber

$$n^2(r) = n_0^2[1 - (\alpha r)^2] \tag{10}$$

for which the propagation constants are given as[1]

[1] In (11) l and m are the azimuthal and radial quantum numbers. The solution corresponding to these numbers is

$$\phi_{lm}(r, \varphi, z, t) = A_{lm}(Kr)^l L_m^{(l)}[(Kr)^2] \exp[-(Kr)^2] \cdot \exp(il\varphi) \exp[i(\beta_{lm} z - \omega t)]$$

where A_{lm} is a normalization constant; $K = [k_0 - n_0\alpha]^{1/2}$ and $L^{(l)}(x)$ are the generalized Laguerre polynomials. The pair of numbers (l, m) is not to be confused with a different pair $-(p, q)$ which is associated with the better known type of solutions

$$\phi_{pq}(r, \varphi, z, t) = A_{pq} H_p(Kx) H_q(Ky) \exp[-(Kr)^2/2] \exp[i(\beta_{pq} z - \omega t)]$$

where

$$\beta_{pq} = n_0 k_0 \left[1 - \frac{2}{n_0 k_0}\alpha(p + q + 1)\right]^{1/2}$$

and $H_p(x)$ is the Hermite polynomial of order p. The smearing length is, of course, independent of the mathematical representation.

$$\beta_{lm} = n_0 k_0 \left[1 - \frac{2}{n_0 k_0}\alpha(l + 2m + 1)\right]^{1/2} \tag{11}$$

is capable of relaying images to a certain distance. If the expression in (11) is expanded in powers of $(2/n_0k_0)\alpha(l + 2m + 1)$ to the first power, then (4) is satisfied and images are formed at distances $L_p = P(2\pi/\alpha)$. But image quality is degraded with distance and is completely smeared at a distance

$$L_{\text{smear}} = \frac{n_0(2\pi)^2}{\lambda_0\alpha^2[l + 2m + 1]^2_{\max}}. \tag{12}$$

Using common notation of $\Delta = [n(0) - n(a)]/n(0)$, where a is the actual radius of the core, we can write

$$[l + 2m + 1]_{\max} = \frac{k_0 n_0 \alpha\sqrt{\Delta}}{\sqrt{2}}. \tag{13}$$

By substitution of (13) into (12), the expression for the smearing length is simplified to yield

$$L_{\text{smear}}(\text{parabolic index}) = \frac{\lambda_0}{n_0}\cdot\frac{1}{\Delta^2}. \tag{14}$$

For $\Delta = 10^{-3}$ and $\lambda = 0.6$ μm, the smearing length is 40 cm. The number of modes that propagate in the fiber $-N$ is given as

$$N = \frac{k_0^2 n_0^2 \Delta^2}{\alpha^2} = \frac{1}{2}k_0^2 n_0^2 a^2 \Delta \tag{15}$$

so that by reducing Δ, it is possible to increase the smearing length, but at the same time the number of modes, which is essentially the number of resolution elements of the transmitted picture, decreases.

In 1969 a group of scientists presented the first parabolic index fiber, known today as the "selfoc" fiber [23], in which they transmitted an image through 1 m. Thereafter, similar large-diameter plastic fibers were produced and tested by another group [24], but the fiber lengths in their experiments were only several centimeters.

Recently, Silberberg and Levy [25] suggested a refractive index profile for which the smearing length is greater than the smearing length of the parabolic index fiber as given by (11). The profile is a modified hyperbolic secant profile of the form

$$n^2(r) = \frac{n_0^2}{\cosh^2(\alpha r)} + \frac{\alpha^2(l_0^2 - 1/4)}{k_0^2}n_1^2(\alpha r)$$

where

$$n_1^2(\alpha r) = \frac{1}{(\alpha r)^2} - \frac{1}{\sinh^2(\alpha r)} - \frac{1}{3\cosh^2(\alpha r)}. \tag{16}$$

For this profile, the family of propagation constants, which have the azimuthal quantum number $l = l_0$, are equally spaced

$$\beta_{l_0,m} = \alpha S - 2\alpha m$$

with

$$S = [k_0^2 n_0^2/\alpha^2 - (l_0^2 - 1)/3]^{1/2} - l_0 - 1. \tag{17}$$

The other propagation constants are shifted slightly according to

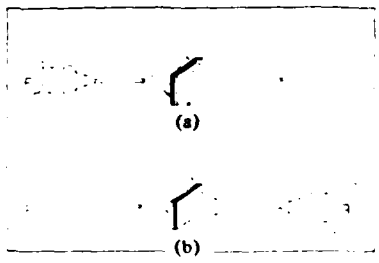

Fig. 2. Holographic phase conjugation filter. (a) Recording arrangement. (b) Readout arrangement.

$$\beta_{lm} = [k_0^2 n_0^2 - \alpha^2(l_0^2 - 1)/3]^{-1/2} - \alpha(l + 2m + 1) + \frac{\alpha^2(l_0^2 - l^2)}{2k_0 n_0}K_{lm} \tag{18}$$

where K_{lm} is a number lower than 0.17. The smearing length for this profile, which is the same as for the hyperbolic secant profile, is

$$L_{\text{smear}}(\text{hyperbolic secant}) = 3\frac{\lambda_0}{n_0}\cdot\frac{1}{\Delta^2} \tag{19}$$

which is greater by a factor of 3 than the smearing length for the parabolic profile as given in (12).

Kawakami and Nishizawa, exploiting ray optics, have shown that the optimal profile for helical rays is [26]

$$n^2(r) = n_0^2[1 + (\alpha r)^2]^{-1} \tag{20}$$

and that the optimal profile for meridional rays is, of course, the hyperbolic secant

$$n^2(r) = n_0^2 \operatorname{sech}^2(\alpha r). \tag{21}$$

Consequently, since the two profiles differ, at least in the ray optics picture, an optimal profile for all rays does not exist. For large diameter fibers (hundreds of times larger than the wavelength of light) the ray optics approach provides a good approximation, thus illustrating that pictures containing a large number of resolution elements cannot be perfectly transmitted by any type of round fiber. So, despite the fact that graded-index fibers provided a partial solution to the image transmission problem, they cannot be used for long distances.

IV. Field Conjugation

An imaging scheme involving phase conjugation, was first suggested by A. Yariv in 1975 [27] and recently demonstrated by G. J. Dunning [28]. In this scheme, a nonlinear optical element is placed between two sections of identical fibers having exactly the same length. The picture field propagates through the first section, undergoes a conjugation transformation by the nonlinear element, and then the conjugate field propagates through the second section. At the output of the second section the field is a conjugate replica of the input picture field. In his paper, Yariv suggested a nonlinear crystal to produce the conjugate field.

Rather than using a nonlinear crystal we exploited a holographic technique for producing the conjugate field. The scheme is illustrated in Fig. 2. The light emerging from the first fiber section interferes with a plane-wave beam, and the pattern is recorded on a photographic plate. After development, the hologram is rotated by 180° and replaced in the

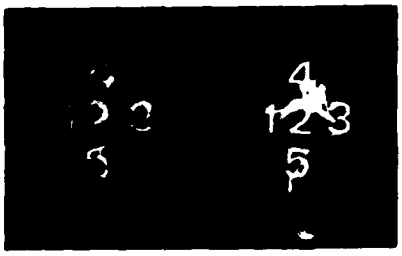

(a) (b)

Fig. 3. Results with holographic phase conjugation filter. (a) Object at input face of fiber. (b) Output imagery.

original location (if the hologram is thin, it is not necessary to rotate the hologram since the conjugate wavefront is reconstructed with a readout plane wave oriented symmetrically with respect to the normal of the hologram plane). The reconstructed conjugate wave propagates through the second fiber section and an image is formed on the end-face of that section. Mathematically, the sequence of transformations that the input picture field undergoes is described as follows:

$$\sum_{l,m} A_{lm}\phi_{lm} \xrightarrow{T_1} \sum_{l,m} A_{lm}\phi_{lm}\, e^{i\beta_{lm}L} \xrightarrow{T_2} \sum_{l,m} A^*_{lm}\phi^*_{lm}\, e^{-i\beta_{lm}L} \xrightarrow{T_3} \sum_{l,m} A^*_{lm}\phi^*_{lm}. \quad (22)$$

The four expressions give the field distribution at the four faces of the fibers from left to right. T_1 and T_3 denote the transformations that result after propagating a distance L through the fiber, and T_2 is the conjugation transformation (including propagation from the end of first fiber section to the hologram and from the hologram to the beginning of the second fiber section).

In our first experiment the holographic setup was so arranged as to allow the reconstructed field to propagate back through the same fiber. A similar experiment to correct the imaging through fibers was done by E. Spitz [29], and analogous experiments were conducted by E. Leith, J. Upatnieks, and A. Van der Lugt to holographically correct lens aberrations [30]. The fiber was a glass rod of 25 cm in length and 0.9 mm in diameter. The results are shown in Fig. 3. In this experiment, one fiber essentially simulates two identical sections so that the results shown in Fig. 3 are rather impressive. In a more practical situation, two different fiber sections must be employed. To test qualitatively the matching tolerances that would be required of the two sections, we performed an experiment with the same setup, except that the fiber was rotated around its axis of symmetry prior to reconstruction and return propagation. In essence, then, only the microstructure of the fiber is different for the forward and backward propagations, but otherwise, the fiber is identical for the two. Representative results are shown in Fig. 4. Fig. 4(a) depicts a photograph of the input object of transparent letters in a dark background. Fig. 4(b), (c), and (d) shows the output after reconstruction and propagation, when the fiber was rotated by 0°, 120°, and 180°, respectively. Clearly, the output imagery has more degradation as the rotation is increased.

The two experiments demonstrate the validity of the concept but, at the same time, also show the dominant pitfalls. In particular, it is unlikely that two identical fibers (including identical microstructure) can be found. Moreover, coherent

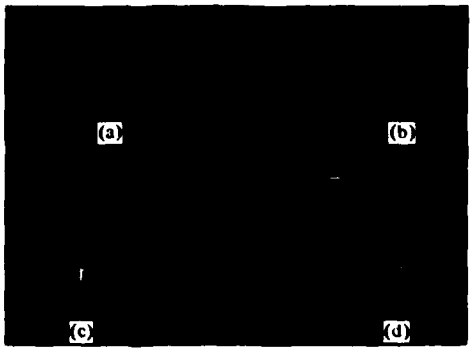

Fig. 4. Holographic reconstruction through an optical fiber as a function of fiber rotation about its axis. (a) Object. (b) Reconstruction with no rotation. (c) Rotated by 120°. (d) Rotated by 180°.

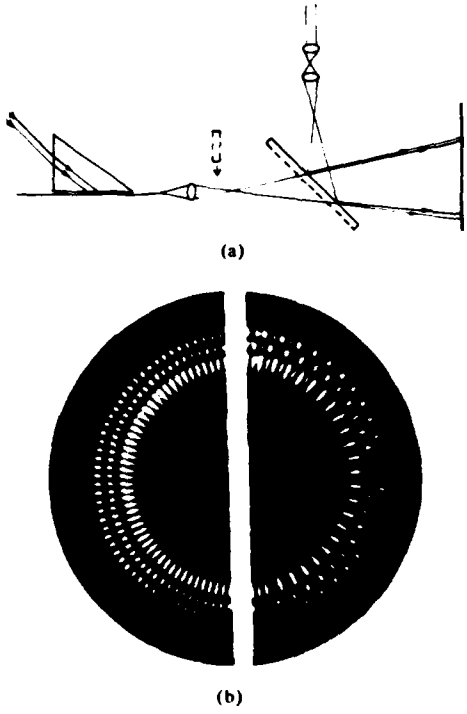

(a)

(b)

Fig. 5. Excitation of leaky fiber modes. (a) Arrangement for coupling light into fiber in order to excite only one mode. (b) Left-half regular mode pattern ($LP_{50,1}$). Right-half interferogram of mode with plane wave.

light sources and good mechanical stability are necessary, and the filter depends on the input picture field.

A simpler technique, which still uses coherent light, is described in the next section. It does not require matching of two fibers but is based on a multiplexed holographic filter for restoring the imagery at the output of the fiber.

V. Composite Hologram Filter

Since the field distribution at the output end of the fiber due to the excitation of a given point at the input face depends strongly on the location of that point, the image transmission arrangement through a single fiber may be regarded as a space variant system. As such, the point spread functions of the individual input points differ from each other, so that no one single filter can restore the smeared output imagery. In this section we present a technique in which a set of composite holographic filters modifies the point spread functions in order to restore the original input image [31].

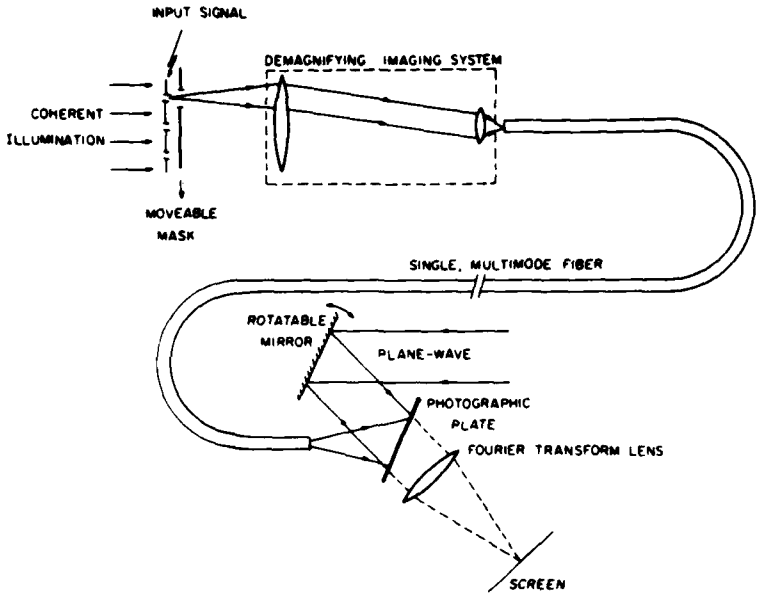

Fig. 6. Optical arrangement for recording a holographic filter and for transmitting pictures through a single fiber.

In this technique the field is independently excited at different points on the input face of the fiber, and the corresponding point spread functions of each point are holographically recorded, each with a differently oriented reference beam. This forms a composite recording of many component holograms each of which can be read out separately by light representing a corresponding point spread function. Thus when the readout light at the output of the fiber, caused by the excitation of a given input point, impinges on the composite hologram, most of the diffracted energy propagates in the direction corresponding to the original reference beam, representing the signal. A small fraction is diffracted to other directions, representing crosstalk noise. Such a multiplexing scheme was suggested by Pennington and Collier [32] for reducing the ghost imagery associated with multicolor holography, and, more recently, by F. Krile, R. J. Marks, J. F. Walkup, and M. O. Hagler [33] to form space variant filters in optical processing.

In order to estimate the signal-to-noise ratio of this scheme, we assume a coherent light excitation at the input face of a step-index fiber of the form

$$E_{1x} = \hat{x} \cdot \delta(r - r_i, \phi - \phi_i) \tag{23}$$

where r_i, ϕ_i are the polar coordinates of the input point. For simplicity we use the "weak guidance" approximation, which leads to LP modes [34]. There are four degenerate orthonormal modes which belong to the same eigenvalue β_{lm}

$$\begin{aligned} \epsilon_{lm1} &= \hat{x} f_{lm}(\rho) \cos(l\phi) \\ \epsilon_{lm2} &= \hat{x} f_{lm}(\rho) \sin(l\phi) \\ \epsilon_{lm3} &= \hat{y} f_{lm}(\rho) \cos(l\phi) \\ \epsilon_{lm4} &= \hat{y} f_{lm}(\rho) \sin(l\phi) \end{aligned} \tag{24}$$

where

$$f_{lm}(\rho) = A_{lm} \begin{cases} J_l(V_{lm}\rho), & \rho < 1 \\ K_l(W_{lm}\rho), & \rho > 1 \end{cases} \tag{25}$$

and $\rho = r/a$ is a normalized radius, a is the core radius, $A_{l,m}$ is a normalization constant, and J_l, K_l are the Bessel and Hankel functions, respectively. V_{lm} and W_{lm} are related to the dimensionless parameter V as

$$V_{lm}^2 + W_{lm}^2 = V^2 = k_0^2 a^2 (n_1^2 - n_2^2).$$

To demonstrate the validity of this approximation, we conducted an experiment in which only one leaky mode was excited. This was achieved by coupling coherent light into the fiber through a prism, as shown in Fig. 5(a). Light from the output end was imaged through a polarizer onto a screen where it interfered with a spherical reference wave having the same radius of curvature. A photograph of the results is shown in Fig. 5(b). The regular mode pattern without the reference wave is shown on the left, whereas the interference pattern is shown on the right. Both the sinusoidal angular dependence and the Bessel radial dependence are evident. Note the change of sign between neighboring peaks both in the radial and azimuthal directions.

Based on the above expressions for the guided modes, the signal-to-noise ratio (SNR) can be calculated. The signal is defined as the diffracted power from a filter which corresponds to a particular incident point, whereas the noise is defined as the power diffracted into the same direction, caused by excitation from the other input points. The calculation is done by expanding each input field into the complete set of fiber modes and using these to evaluate the diffracted fields from the holographic filters. This calculation is rather cumbersome, so we only present the final result

$$S/N \simeq 2N_F/N_P \tag{26}$$

where N_F is the number of nondegenerate modes and N_P is the number of different input points in the composite filter. In the derivation we assumed an ideal straight fiber (neglecting scattering) and an ideal material for recording the holographic filter.

The experimental arrangement for recording the composite holographic filter, as well as for transmitting two-dimensional information through a single fiber is shown in Fig. 6. An array of pinholes is projected onto the input face of the fiber

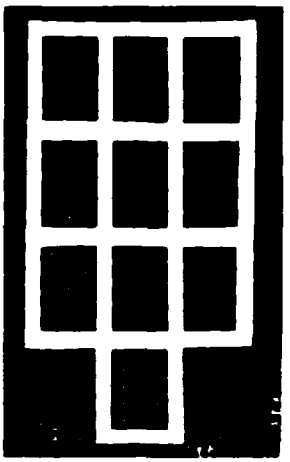

Fig. 7. Experimental results of the transmitted ten decimal digits.

by a demagnifying lens system. In recording, light from only a single pinhole selected by a moveable mask falls on the input face of the fiber at a time. At the output end, the point spread function (after magnification) is holographically recorded with a certain orientation of the reference beam. Next, after translating the moveable mask to another position and changing the orientation of the reference by means of a deflecting mirror, a new hologram is superimposed on top of the previous one. This process continues for all pinholes in the input array to form the composite hologram filter. In a specific experiment the input array consisted of 13 pinholes in the form of a seven-bar diagram. The waveguide was step-index round plastic fiber of 60-cm length and 0.8-mm diameter. The recording material was a photodielectric polymer capable of *in situ* development [35], and having sufficient dynamic range to handle the 13 superimposed holograms.

After recording the filter, light through selected pinholes was blocked so as to form a pattern of a decimal digit, for transmission. At the output end the diffracted light from the filter is collected by a Fourier transform lens to form a small spot at the focal plane for each input point. The experimental output images are shown in the photographs in Fig. 7. As shown, the SNR is high, since the noise was well below the threshold of the output recording films, clearly demonstrating the effectiveness of the technique; the one-to-one correspondence which exists between input and output points is clearly evident in spite of the fact that the transmission is through a space varying system. In other words, each point spread function is primarily affected by its conjugate filter and not so much by the other, superimposed filters.

The dynamic range requirement may be relaxed by changing the excitation and recording scheme. For example, a plane-wave at the input face excites only a group of modes which, emerging from the output end, propagate in a narrow conical shell [36]. As a consequence, one recording plate can serve for recording spatially separated and independent holograms, thereby decreasing the number of superimposed holograms at any given area of the plate. With such a recording scheme, the number of input sampling points may be considerably enlarged.

As a final note, we would like to point out that the SNR is essentially independent of the length of the fiber, as long as the fiber remains dimensionally stable.

VI. Multiplexing

Thus far we have considered techniques in which smearing was overcome either by changing the fiber geometry or by introducing a phase compensation filter at the output end of the fiber. In this section we shall consider techniques in which both the input and the output are involved. Specifically, we shall describe methods in which optical components at the input encode the spatially modulated light so that the information is not scrambled during propagation, and optical components at the output decode the information to form the original spatial pattern.

There are three coordinates that are not mixed by the fiber, axial angle θ, wavelength λ, and time t. Thus if a ray of light with these three coordinates $(\theta_1, \lambda_1, t_1)$ is introduced into the fiber, it will emerge from the output end with the same set of coordinates, except for a constant delay added to the time coordinate $(\theta_1, \lambda_1, t_1 + T)$. Consequently, in order to transmit a two-dimensional picture through a single fiber, it is first necessary (and of course sufficient) to transform the two spatial coordinates of the picture into any combination of two of the three coordinates mentioned above, then to let the light propagate through the fiber, and finally to retransform in order to obtain the image of the original picture. These transformations and retransformations are usually referred to as multiplexing and demultiplexing, respectively.

In the following we consider several optical arrangements in which one or two forms of multiplexing are used for transmitting two-dimensional imagery through a single fiber. Prior to describing these systems and the experimental results, we consider the angular multiplexing technique separately because it is the least familiar of the three schemes.

A. Axial-Angle Multiplexing

The underlying principle for transmitting the angular coordinate by multiplexing is based on the fact that the angle between the propagation direction of a ray of light and the symmetry axis of a step-index fiber is kept unchanged as the ray bounces from the core-clad interface [36]. As proof, consider a ray propagating in the direction $\boldsymbol{k} = (k_x, k_y, k_z)$. The axial angle θ is given by $\cos\theta = k_z/|\boldsymbol{k}|$. The magnitude of the vector $\boldsymbol{k}$ is obviously unchanged by reflection, and we want to show that the same is true for k_z. Now, the relation between the propagation constant of an emerging beam, $\boldsymbol{k}(\text{out})$, and that of an incoming beam, $\boldsymbol{k}(\text{in})$, due to reflection from a certain plane is given by a reflection matrix (R) as $\boldsymbol{k}(\text{out}) = (R)\boldsymbol{k}(\text{in})$. Describing the plane by a unit vector $\hat{n} = (n_x, n_y, n_z)$ perpendicular to the plane, it is known [37] that

$$(R) = \begin{pmatrix} 1 - 2n_x^2; & -2n_x n_y; & -2n_x n_z \\ -2n_x n_y; & 1 - 2n_y^2; & -2n_y n_z \\ -2n_x n_z; & -2n_y n_z; & 1 - 2n_z^2 \end{pmatrix} \tag{27}$$

yielding for $n_z = 0$

$$(R)_f = \begin{pmatrix} 1 - 2n_x^2; & -2n_x n_y; & 0 \\ -2n_x n_y; & 1 - 2n_y^2; & 0 \\ 0; & 0; & 1 \end{pmatrix}. \tag{28}$$

All the reflections inside the fiber are described by matrices of the type $(R)_f$ for which $n_z = 0$. Clearly, with such matrices $k_z(\text{out}) = k_z(\text{in})$, and this equality completes the proof.

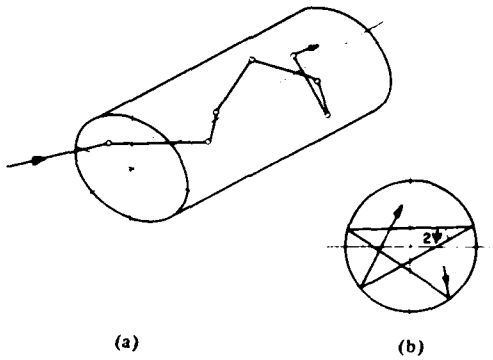

(a) (b)

Fig. 8. Ray geometry in fiber. (a) General ray path. (b) Cross-sectional view defining the angle ψ.

The azimuthal angle, on the other hand, is not preserved. In fact, when a plane wave excites all rays with a given azimuthal (and axial) direction of propagation, the light rays emerging from the fiber will make a conical shell having a uniform density around the cone. As a result of these two effects -axial angle preservation and density uniformity in the azimuthal angle-the light pattern on a screen, some distance away from the output end, is a narrow, uniform ring. To show the azimuthal uniformity, consider a ray whose azimuthal input angle is $\phi_{in} = 0$. The azimuthal angle at the output, is $\phi_{out} = n(\psi)[2\psi - \pi]$, with ψ defined in Fig. 8. The number of reflections, $n(\psi)$, is $n(\psi) = L \tan\theta/2a \cos\psi$. Around $\psi = 0$ and for small θ, $n(\psi) = (L\theta/2a)[1 + (1/2)\psi^2]$. The angle, ψ_1, for which the number of reflections $n(\psi_1)$ is increased by 1, compared to the number of reflections at $\psi = 0$, is $\psi_1 = [4a/L\theta]^{1/2}$. On the other hand, the change in azimuthal angle of the emerging beam is

$$\Delta\phi_{out} = \phi_{out}(\psi_1) - \phi_{out}(0) = 2(L\theta/a)^{1/2}. \quad (29)$$

For $L = 25$ m, $a = 600$ μm, and $\theta = 0.1$ rad, $\psi_1 = 1.2°$ and $\Delta\phi = 29 \times 360°$. It means that if the angle ψ is changed continuously from 0° to 1.2°, the rays emerging from the fiber will continuously circle the output ring 29 times. For any small interval in ψ the output azimuthal density is independent of ψ and the same is, of course, true for the sum.

A more accurate calculation of the far-field output pattern from a multimode step-index fiber, due to oblique plane-wave excitation, can be given in terms of guided modes. A plane wave, which is launched at an axial angle θ into the fiber, is expanded into the guided modes. Each of these modes propagates to the exit end of the fiber with the proper propagation constant, and the far-field pattern can be calculated. This derivation is rather cumbersome, but the main result is that only modes with (l, m) given by

$$l + 2m = \frac{2}{\pi} k_0 n_1 a \sin\theta \quad (30)$$

are strongly excited, while all other modes are virtually absent. The far-field pattern which is obtained from these modes is circularly symmetric. The radial part peaks at θ, and is very much like a diffraction pattern from a circular aperture having a maximum intensity which coincides with the maximum predicted by ray tracing.

In the angular multiplexing experiments, we have used an optical setup similar to the one shown in Fig. 9. Light is modulated by the signal along a narrow slit placed at the back focal plane of a lens. The spatially modulated light is decomposed by the lens into a set of plane waves each having a unique direction of propagation. The light propagates through the fiber and forms on a screen a pattern whose radial dependence is a copy of the modulating signal along the input slit. Figs. 10 and 11 display our results with a 25-cm-long fiber. The input signal is shown on the left, and the output pattern is shown to the right. These results confirm the preceding discussion and show that indeed the axial angle is an unmixed coordinate and (together with either time or wavelength coordinate) forms the basis for two-dimensional image transmission through a single step-index fiber.

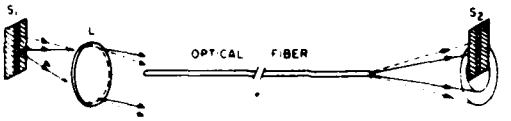

Fig. 9. Basic arrangement for angular multiplexing and transmission.

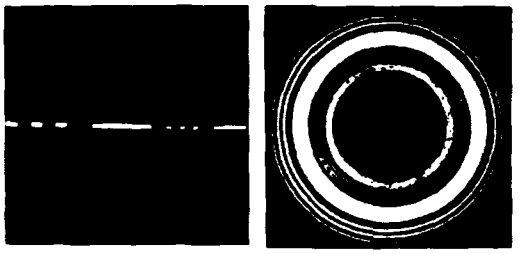

(a) (b)

Fig. 10. Binary signal transmission with angular multiplexing. (a) Binary input. (b) Corresponding output pattern.

(a) (b)

Fig. 11. Continuous tone signal transmission with angular multiplexing. (a) Input. (b) Corresponding output pattern.

In the following section we present the experimental arrangements and results obtained for each of the three multiplexing combinations: 1) θ-t multiplexing; 2) θ-λ multiplexing; and 3) λ-t multiplexing. The discussion of picture quality, mainly in terms of the number of resolution elements carried by each of the three coordinates, is given in a separate section following the presentation of experimental results.

B. Experimental Procedure and Results

1) Angular-Time (θ-t) Multiplexing: In the angular-time multiplexing image transmission scheme the two-dimensional light signal is transformed into the axial angle and time coordinates. The optical setup for performing this transformation (and the inverse transformation at the other end of the fiber)

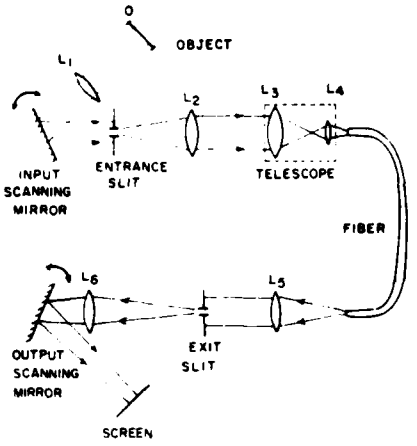

Fig. 12. Optical arrangement for multicolor picture transmission by angular-time multiplexing.

is shown in Fig. 12. The information bearing transparency is imaged through a moveable mirror onto the entrance slit which selects one line to be transmitted. The light emerging from the slit is decomposed into plane waves by lens L_2 and the angular span of the plane waves is magnified by the L_3-L_4 lens combination. After propagation through the fiber, the light is collected by lens L_5 to form a circularly symmetric pattern at the plane of the exit slit. The radial line from the pattern is selected by the slit and an image of the intensity variations along that line falls at a certain location on the output screen by means of the imaging lens L_6 and the output scanning mirror. When the two mirrors rotate synchronously, an image of the two-dimensional input transparency is formed on the screen. In order to increase the light collection efficiency, it is possible to include annular mirrors behind lens L_5, each of which collects and deflects the light of a given ring by a specific angle into the slit [38]. Alternatively, if coherent light is employed, the mirrors can be replaced with holographic optical elements.

Some representative results obtained with the optical arrangement of Fig. 12 are shown in Figs. 13 and 14; these illustrate the effectiveness of the angular-time multiplexing technique for transmitting pictorial data by a single, step-index, round fiber. The output imagery, for which a standard resolution chart served as the object, is shown in Fig. 13. The transparency of the chart was illuminated with monochromatic laser light, and the image was transmitted through a 25-cm-long fiber rod of 0.9-mm diameter. In Fig. 13(a) we focus on the details of pattern number 1 where the asymmetry in resolution is evident; while the three vertical lines 1-6 (3.56 line-pairs/mm) are clearly resolved, the horizontal lines of the same level are barely resolved. Because of a limited field of view, a second photograph Fig. 13(b) is needed to show the details of pattern number 2; here the vertical lines of levels 2-6 (7.13 line-pairs/mm) are still resolved.

Fig. 14 shows the results of transmitting the image from an object transparency, consisting of transparent letters against a dark background, through a 25-m-long step-index fiber of 600-μm diameter; the illumination source was a 75-W xenon arc lamp. A photograph of the signal at the input face of the fiber is shown in Fig. 14(a), and the corresponding transmitted image in Fig. 14(b).

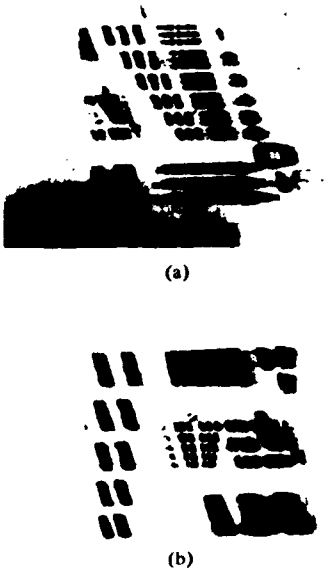

Fig. 13. Resolution target imaged through a fiber rod by angular-time multiplexing for two different fields of view. (a) Level 1-6 horizontal lines are barely resolved. (b) Vertical lines at levels 2-6 are still discernible.

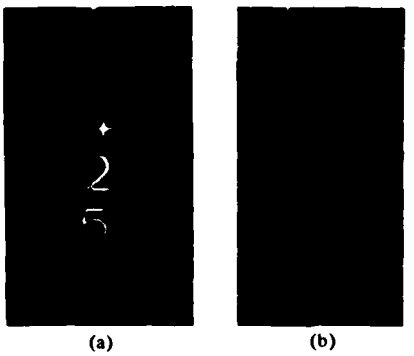

Fig. 14. Image transmitted through a 25-m-long, step-index fiber by angular multiplexing. (a) Input. (b) Output.

2) Angular-Wavelength (θ-λ) Multiplexing: By replacing time multiplexing with wavelength multiplexing, and again combining it with angular multiplexing, it is possible to obtain a completely passive system for transmitting in parallel an entire two-dimensional picture through a single fiber. The wavelength multiplexing is achieved by coding each line of a two-dimensional picture with a different color illumination. In practice, this coding is implemented by means of a dispersive element, such as a prism or a grating, which disperses white light into various color strips, each illuminating a different area of an input transparency. The information from each of the color-coded strips is transmitted and detected by means of angular multiplexing as before, but at the output, additional optical elements distinguish one strip from another and rearrange the strips according to their original relative positions.

The imaging technique is implemented by the optical arrangement shown in Fig. 15. The input coding slit S_1 is at the back focal plane of lens L_1 and is illuminated with a white light source. A prism, P_1, disperses the light into its spectral com-

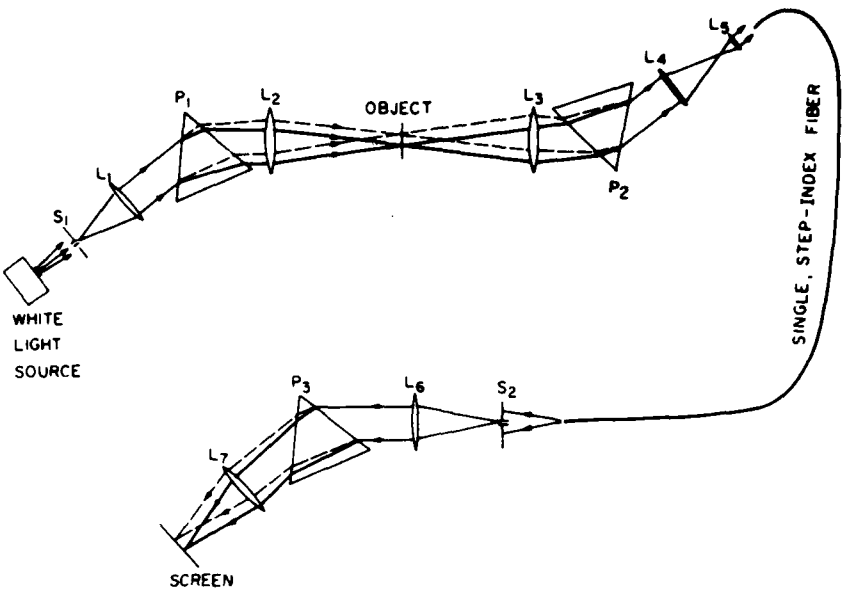

Fig. 15. Optical arrangement for two-dimensional imagery by angular-wavelength multiplexing.

ponents, each passing through a second lens L_2, thereby forming multiple images of the slit, each of a different color, at the front focal plane of L_2. Each line of the object transparency located at that plane is thus encoded with a different wavelength. Lens L_3 decomposes the light signal along every line of a certain color into plane waves as required for angular multiplexing. Prism P_2 recollects the light of all colors, and after angular magnification by lenses L_4 and L_5, the light is introduced into the fiber. After transmission through the optical fiber, a second slit S_2 selects one line (containing all colors) from the emerging circularly symmetric far-field pattern. The light from the slit is collected by the collimating lens, L_6, and the resultant output beam is then dispersed by the prism, P_3. Finally, lens L_7 refocuses the dispersed light onto a screen to form an exact replica of the input signal. By juxtaposing Fig. 12 and Fig. 15, it becomes evident that the prisms P_1 and P_2 of Fig. 15 play a role which is very similar to that of the input and output scanning mirrors of Fig. 12. In fact, the time and wavelength coordinates are analogous in several respects, some of which are discussed in a subsequent section.

In the experiments, the illumination source was a 75-W xenon arc lamp, the input transparency consisted of transparent letters against a dark background, and the optical guide was a 15-m-long step-index, multimode fiber of 600-μm diameter. A representative result of the output imagery obtained with the arrangement of Fig. 15 is shown in Fig. 16. The resolution in the x direction is determined by the slits which were normally 200 μm wide, so as to give about 5 line-pairs/mm. In the y direction, the resolution depends on both the fiber characteristics and angular magnification of the input optics, and for our system was about 2 line-pairs/mm.

3) Wavelength-Time (λ-t) Multiplexing: The method of image transmission by the wavelength-time multiplexing is conceptually simple and relatively easy to implement experimentally. As in the preceding section, we shall again emphasize the wavelength multiplexing part. For the wavelength-

Fig. 16. Image transmitted through a 15-m-long fiber by angular-wavelength multiplexing.

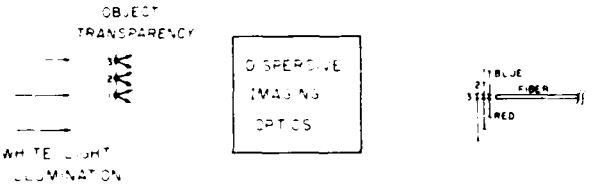

Fig. 17. Schematic arrangement for wavelength multiplexing.

time multiplexing, the optical arrangement of Fig. 15 can be simplified by completely removing the input and output slits and illuminating the object directly with white light. The principle of such an arrangement is schematically illustrated in Fig. 17. The object, which is illuminated with white light, is imaged onto the input face of the fiber by means of an optical system which contains a dispersive element. As a result of the dispersion, light of only a narrow spectral band from each point is collected onto the input face of the fiber, thereby encoding each point with a different wavelength. An obvious implication of this technique is that the fiber diameter dictates the resolution.

The more complete optical arrangement, in which the auxiliary slits have been essentially replaced with the optical fiber itself, is shown in Fig. 18. The object is imaged onto the input face of the fiber by means of lenses L_1 and L_2. This image, however, is spectrally smeared by the dispersive element positioned between the two lenses. In our experiments,

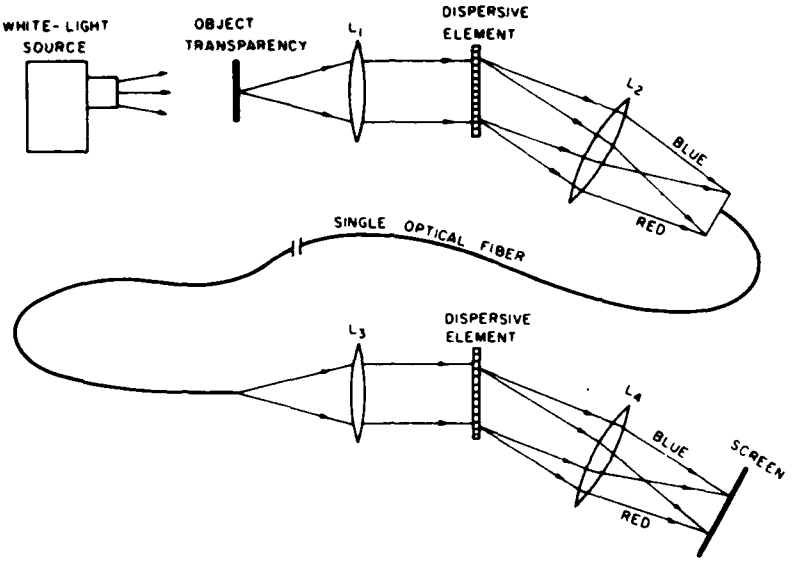

Fig. 18. Optical arrangement for transmitting black and white pictures through arbitrarily long and curved optical fiber by the wavelength-time multiplexing.

Fig. 19. Image transmitted through a 25-m-long fiber by wavelength-time multiplexing.

holographic gratings served as the dispersive elements since they have dispersion powers which are much greater than those of conventional prisms. Therefore, lenses with shorter focal lengths are adequate for transmitting a given number of resolution elements, making the system more compact. Finally, the input face of the fiber determines the smaller area, from which light is collected into the fiber. At this area each point along one line of the object contributes light of a specific color so that one-dimensional wavelength multiplexing is achieved.

The time multiplexing is implemented with two synchronously scanning mirrors (not shown in the drawing) which are placed near the dispersion elements. Indeed, the configuration stresses the similarity between the wavelength and time coordinates. The wavelength multiplexing arrangement shown in Fig. 17 is obviously simpler than the one shown in Fig. 15; moreover, it more closely resembles the practical situation in which the object is illuminated directly with white light rather than an encoded wavelength illumination. However, the light collection efficiency of the arrangement shown in Fig. 17 is inferior to that of Fig. 15.

Fig. 19 shows a photograph of an image transmitted through a 25-m-long fiber having 200-μm diameter. The picture contains about 120 by 140 resolution elements. Except for some minor scatter losses, the picture quality is not affected by the length of fiber. Indeed, we obtained comparable results with 500-m-long fibers [39].

C. Discussion

The most important parameter for characterizing the quality of the transmitted pictures is the number of resolution elements. Other relevant parameters include the magnification, field of view, and the size of the pictures. In this section we shall consider these parameters for the three multiplexing configurations.

We begin with the angular multiplexing scheme in which the number of resolution elements is directly related to the spreading of the beams which emerge from the fiber. This spread is, in general, a function of the axial angle of the incident and emerging beams, and we designate it as $\sigma(\theta)$. Refer to Fig. 12, and let x_1 and x_2 denote the coordinates along the entrance and exit slits, respectively. The relation between the axial angle θ and x_1 is given approximately as

$$x_1 = \xi\theta, \quad \text{with } \xi = \frac{f_2 f_4}{f_3} \tag{31}$$

where f_2, f_3, and f_4 are the focal lengths of lens L_2, L_3, and L_4, respectively. Now, the resolution R (i.e., the distance along the entrance slit between two resolvable adjacent points), the magnification M, and the field of view $x_1(\max)$ are given as

$$R_1(x_1) = \xi\sigma(x_1), \quad M \equiv \frac{x_2}{x_1} = \frac{f_3 f_5}{f_2 f_4}, \quad x_1(\max) = \xi\theta_c \tag{32}$$

where θ_c is the critical angle characterizing the fiber. The number of resolution elements is thus given as

$$N_\theta = \int_0^{x_1(\max)} \frac{dx_1}{R_1(x_1)} = \int_0^{\theta_c} \frac{d\theta}{\sigma(\theta)}. \tag{33}$$

For an ideal straight fiber having a radius a, the width of the spread $\sigma(\theta)$ is essentially derived from diffraction considerations and is given, approximately, as $k_0 n_0 a\sigma(\theta) \simeq \pi$. For

$n_0 = 1$, the width of the diffraction limited angular spread is thus $\sigma = \lambda/2a$. Since this spread is not dependent on θ, we obtain from (33) that the upper limit of the number of resolution elements is

$$N_\theta(\text{upper limit}) = 2\theta_c \cdot \frac{a}{\lambda}. \tag{34}$$

If, for example, θ_c (outside the fiber) is 0.5 rad, the radius of the fiber is 300 μm, and λ is 0.6 μm, then N_θ is 500, which is comparable to one line of a television picture. In practice, however, the fibers are not ideal, resulting in greater angular broadening and, consequently, lesser resolution elements.

The two major sources for angular broadening are: 1) coupling between modes due to surface roughness, refractive index irregularities, and microbendings, and 2) coupling between modes due to large bends along the length of the fiber. The first source of coupling is usually characterized by a coupling constant D having a typical value of 10^{-6} rad^2 m. The angular width σ depends on fiber length z as [38], [40]

$$\sigma = [4Dz + \sigma_0^2]^{1/2} \tag{35}$$

where σ_0^2 is the initial width and has, of course, a zero value in the case of plane-wave excitation. Thus for plane-wave excitation, N_θ is given by

$$N_\theta = \frac{\theta_c}{[4Dz]^{1/2}} \tag{36}$$

where the number of resolution elements decreases as the square root of distance. For $z = 25$ m, $\theta_c = 0.5$, and $D = 10^{-6}$ rad^2 m, we obtain $N_\theta = 50$, which is an order of magnitude less than the upper limit.

When the mode coupling is caused by macrobending, the angular spread of meridional rays resulting from a single bend with a radius of curvature R is given by

$$\Delta\theta(\theta) = \pm\arcsin\left\{\frac{1}{2}\left[\sin^2(2\theta) + 8\left(\frac{2a}{R}\right)\cos^2\theta\right]^{1/2} - \frac{1}{2}\sin(2\theta)\right\}. \tag{37}$$

The width $\sigma(\theta)$ is actually smaller than $\Delta\theta(\theta)$, but it is approximately proportional to $\Delta\theta(\theta)$. In our experiments we found that $\sigma(\theta)$ is indeed a function of θ, where it continues to decrease as the angle increases. An additional cause for this decrease is attributed to the change in coupling coefficients as a function of axial angle [41].

In summary, the quality of pictures transmitted by the angular multiplexing technique depends on the diameter and length of the fiber, the number of bends along the fiber, and the coupling coefficient. Such dependence is essentially avoided in the time and wavelength multiplexing schemes, leading to improved picture quality.

We will now derive expressions for the wavelength multiplexing technique illustrated in Fig. 18 in which the magnification, resolution, and number of resolution elements are given as a function of the focal length of the four lenses f_1, f_2, f_3, and f_4; the dispersion power of the two dispersive elements—A_1 and A_2 (defined below), the diameter of the fiber d (assuming the fiber has the same diameter at both ends); and the available bandwidth B. After some slight modification, we shall show that these expressions are also valid for the time multiplexing technique.

With reference to Fig. 18, consider the x coordinate at four different planes, which coincide with either the front or the back focal plane of the various lenses: x_1—at the object plane; x_2—at the plane of the fiber's input face; x_3—at the plane of the fiber's output face; and x_4—at the image plane. Also the dispersion power at λ_0 of the dispersive elements is defined as

$$A \equiv \left.\frac{d\theta}{d\lambda}\right|_{\lambda=\lambda_0}. \tag{38}$$

Now the angular deviation of the beam at each wavelength can be expressed in a Taylor series as

$$\theta(\lambda) = \theta(\lambda_0) + A(\lambda - \lambda_0) + \frac{1}{2!}\frac{d^2\theta}{d\lambda^2}(\lambda - \lambda_0) + \cdots. \tag{39}$$

If we assume that λ_0 is the center of the spectral bandwidth and that all the lenses are perpendicular to the beam of λ_0, then $\theta(\lambda_0) = 0$. By neglecting higher order terms (which represent distortions and introduce unnecessary complications to the calculations), it is possible to use the paraxial approximation to obtain

$$x_2(x_1, \lambda) = -\frac{f_2}{f_1}[x_1 - A_1 f_1(\lambda - \lambda_0)] \tag{40}$$

and similarly

$$x_4(x_3, \lambda) = -\frac{f_4}{f_3}[x_3 - A_2 f_3(\lambda - \lambda_0)]. \tag{41}$$

Using (40) and (41), the magnification is found to be

$$M \equiv \frac{x_4}{x_1} = \frac{f_4}{f_1}\frac{A_2}{A_1}. \tag{42}$$

In the configuration under discussion, the magnification is not affected by the focal lengths of lenses L_2 and L_3. The resolution R_1, namely, the smallest distance between two resolvable lines in the object plane, is

$$R_1 = df_1\left[\frac{1}{f_3}\frac{A_1}{A_2} + \frac{1}{f_2}\right]. \tag{43}$$

For a given bandwidth B (dictated either by the bandwidth of the source or that of the detector) the spatial extent of the object is bounded as

$$-\tfrac{1}{2}A_1 f_1 B \leqslant x_1 \leqslant \tfrac{1}{2}A_1 f_1 B \equiv x_1(\max). \tag{44}$$

From (43) and (44), the number of resolution elements N_λ is found to be

$$N_\lambda = \frac{B}{d}\left[\frac{1}{A_1 f_2} + \frac{1}{A_2 f_3}\right]^{-1}. \tag{45}$$

We thus see that the parameters of lens L_1 affect the resolution and the field of view, but the number of resolution elements (for a given bandwidth and fiber's diameter) depends solely on the focal lengths of L_2 and L_3 and on the dispersion power of the two dispersive elements. The role of L_4 is only to alter the scaling.

By letting $A_1 = A_2 \equiv A$ and $f_2 = f_3 \equiv f$, then (45) reduces to

$$N_\lambda = \frac{1}{2d} \cdot BAf = \frac{x_1(\max)}{d}. \tag{46}$$

The number of resolution elements is proportional to the bandwidth, the dispersion power, and the focal lengths of the lenses at either side of the fiber. It can easily be increased (by increasing f, for example) but at the expense of light flux reduction at the image plane which is inversely proportional to N_λ. Hence, the number of resolution elements is noise limited, of which shot noise is the dominant contributor.

The same expressions are obtained for the time multiplexing scheme where the dispersive elements are replaced with scanning mirrors. The necessary substitutions are

$$A_{1,2} \rightarrow \frac{1}{2} W_{1,2} = \frac{1}{2} \frac{d\theta_{1,2}}{dt} \tag{47}$$

where θ is the angular position of the mirror and

$$B \rightarrow 4\tau. \tag{48}$$

The term τ denotes the time during which the mirror rotates from one extreme angle to the other, assuming constant angular velocity. Thus the number of resolution elements in the time multiplexing N_t can be written as

$$N_t = \frac{2\tau}{d} \left[\frac{1}{W_1 f_2} + \frac{1}{W_2 f_3} \right]^{-1}. \tag{49}$$

As expected, (49) closely resembles (45), showing the similarity between wavelength and time multiplexing.

Finally, we would like to emphasize that, unlike that in the angular multiplexing scheme, the resolution in both the wavelength multiplexing and the time multiplexing is independent of the length of the fiber. Thus these latter two schemes are the most suitable for long-distance image transmission.

VII. Summary and Conclusions

When two-dimensional images are transmitted directly by a single optical fiber, the output imagery is invariably smeared. This smearing is brought about by the phase-velocity dispersion of the fiber modes that are excited by the picture field. In order to overcome the smearing problem, we consider three different types of solutions that allow image transfer through a single fiber: a) control of the fiber's refractive index profile; b) incorporation of complex filters (provided coherent light is used); and c) encoding the information at the input and decoding the output after transmission.

First, we noted that fibers having a parabolic profile of the refractive index are capable of image transfer. However, the imaging distance is limited, typically to 1 m, due to the difference in phase velocities of the various modes supported by the fiber. We also considered a modified hyperbolic secant profile in which the imaging distance could be increased by a factor of three, but still it is too short for most applications.

We then investigated various complex filters compensation filter, conjugation filter, and correlation filter. Conceptually, the compensation filter is a phase filter which is placed at the far end of the fiber and compensates for the phase delay of each mode separately. The conjugation filter is a complex filter placed between two identical fiber sections which reverses the phase relations of the modes acquired while propagating through the first section. As the modes propagate through the second section, the phase differences become smaller and disappear at the far end. The correlation filter directs the outcoming wavefronts, each excited at a different input point, to a preselected location so as to form an undistorted output imagery. Based on our investigations of the properties of the normal modes of a step-index fiber, we show that a compensation filter is not a suitable solution. On the other hand, the conjugation and correlation filters are more useful, as was confirmed experimentally. However, since these filters compensate mainly for phase distortions, a high degree of geometrical stability is required, which often cannot be met in practice.

The most promising techniques involve multiplexing methods. Here the input data are first transformed into intensity variations of coordinates that are not mixed as the light propagates through the fiber. Then, at the far end, an inverse transformation restores the original spatial intensity variations of the input. The unmixed coordinates are the axial angle that a light ray makes with respect to the fiber's axis of symmetry, the wavelength of the light, and the time at which light enters the fiber. Any combination of two of these three is sufficient to transmit two-dimensional imagery through single fibers. The three available different multiplexing combinations have been investigated and supportive experimental results obtained. We have succeeded in transmitting undistorted pictures through single fibers of lengths ranging to 500 m. The number of resolution elements in the pictures ranges from 20 to 160 in each direction. These methods are reliable and easy to implement and therefore may be of practical use.

We expect that as the multiplexing techniques for parallel image transmission evolve, they will replace the more common sequential scheme for transmission in some applications.

Acknowledgment

We are indebted to A. M. Tai, I. Cindrich, L. M. Peterson and S. Shtrikman for many fruitful discussions and for their review of the text.

References

[1] K. C. Kao and G. A. Hockham, "Dielectric-fiber surface waveguide for optical frequencies," *Proc. Inst. Elec. Eng.* (London), vol. 133, pp. 1151-1158, July 1966.
[2] J. L. Baird, "An improved method of and means for producing optical images," Brit. Patent 285 738, Feb. 1928.
[3] N. S. Kapany, "High resolution fiber optics using sub-micron multiple fibers," *Nature*, vol. 184, pp. 881-883, Sept. 19, 1959.
[4] W. P. Siegmund, "Method of making fiber optical image transfer device," U.S. Patent 3 279 903, May 1961.
[5] D. Marcuse, *Theory of Dielectric Optical Waveguides*. New York: Academic Press, 1974.
[6] A. Gover, C. P. Lee, and A. Yariv, "Direct transmission of pictorial information in multimode optical fibers," *J. Opt. Soc. Am.*, vol. 66, pp. 306-311, Apr. 1976.
[7] N. S. Kapany and J. J. Burke, *Optical Waveguides*. New York: Academic Press, 1972.
[8] H. F. Talbot, "Facts relating to optical science," *Philos. Mag.*, vol. 9, p. 401, 1836.
[9] Lord Rayleigh, "On copying diffraction gratings and on some phenomena connected therewith," *Philos. Mag.*, vol. 11, p. 196, 1881.
[10] Yu. N. Denisyuk, N. M. Ramishvili, and U. V. Chavchanidze, "Production of three dimensional images of two dimensional objects without lenses or holography," *Opt. Spectrosc.* (USSR), vol. 30, pp. 603-605, 1971.
[11] J. T. Winthrop and C. R. Worthington, "Theory of Fresnel images-I. Plane periodic objects in monochromatic light," *J. Opt. Soc. Am.*, vol. 55, pp. 373-381, Apr. 1965.
[12] O. Bryngdahl, "Image formation using self-imaging techniques," *J. Opt. Soc. Am.*, vol. 63, pp. 416-419, Apr. 1973.
[13] R. Ulrich, "Image formation by phase coincidence in optical waveguides," *Opt. Commun.*, vol. 13, pp. 259-264, Mar. 1975.

[14] O. Bryngdahl and W. Lee, "On light distribution in optical waveguides," *J. Opt. Soc. Am.*, vol. 68, pp. 310-315, Mar. 1978.
[15] R. Ulrich and G. Ankele, "Self-imaging in homogeneous planar optical waveguides," *Appl. Phys. Lett.*, vol. 27, pp. 337-339, Sept. 1975.
[16] E. T. Kornhauser and A. D. Yaghjian, "Modal solution of a point source in a strongly focusing medium," *Radio Sci.*, vol. 2, pp. 299-310, Mar. 1967.
[17] A. L. Mikaelyan, *Dokl. Akad. Nauk.* (USSR), vol. 81, p. 569, 1951, and A. L. Mikaelyan, "Selfoc dielectric waveguides," *Soviet J. Quant. Electron.*, vol. 7, pp. 266-267, Feb. 1977.
[18] A. Fletcher, T. Murphy, and A. Young, "Solutions of two optical problems," *Proc. Royal Soc.*, vol. 223, pp. 216-225, Apr. 1954.
[19] R. K. Luneberg, *Mathematical Theory of Optics.* Berkeley: University of California Press, 1964.
[20] S. Kawakami and J. Nishizawa, "Kinetics of an optical wave packet in a lens-like medium," *J. Appl. Phys.*, vol. 38, pp. 4807-4811, Nov. 1967.
[21] L. O. Landau and E. M. Lifshitz, *Quantum Mechanics: Non-Relativistic Theory.* New York: Pergamon, 1965.
[22] D. Marcuse, *Light Transmission Optics.* New York: Van Nostrand, Reinhold, 1972.
[23] T. Uchida, M. Furukawa, I. Kitano, K. Koizumi, and H. Matsumura, "A light-focusing fiber guide," *IEEE J. Quantum Electron.* (Abstract), vol. QE-5, p. 331, June 1969.
[24] Y. Ohtsuka, T. Senga, and H. Yasuda, "Light-focusing plastic rod with low chromatic aberration," *Appl. Phys. Lett.*, vol. 25, pp. 659-661, Dec. 1974.
[25] Y. Silberberg and U. Levy, "Modal treatment of an optical fiber with a modified hyperbolic secant index distribution," *J. Opt. Soc. Am.*, vol. 69, pp. 960-963, July 1979.
[26] S. Kawakami and J. Nishizawa, "An optical waveguide with the optimum distribution of the refractive index with reference to waveform distortion," *IEEE Trans. Microwave Theory and Techniques*, vol. MTT-16, pp. 814-818, Oct. 1968.
[27] A. Yariv, "Three-dimensional pictorial transmission in optical fibers," *Appl. Phys. Lett.*, vol. 28, pp. 88-89, Jan. 1976; and A. Yariv, "On transmission and recovery of three-dimensional image information in optical waveguides," *J. Opt. Soc. Am.*, vol. 66, pp. 301-306, Apr. 1976.
[28] G. J. Dunning, "Demonstration of image transmission through fibers by optical phase conjugation," presented at the Conference on Lasers and Electro-Optics, CLEO '82 (Phoenix, AZ, April 16, 1982).
[29] E. Spitz and A. Wertz, "Transmission Des Images a Travers une Fibre Optique," *C. R. Acad. Sci.* (Paris), vol. 264, pp. 1015-1018, Apr. 1967.
[30] E. N. Leith, J. Upatnieks, and A. Van der Lugt, "Correction of lens aberrations by means of holograms," *Appl. Opt.*, vol. 5, pp. 589-593, Apr. 1966.
[31] U. Levy and A. A. Friesem, "Direct picture transmission in a single optical fiber with holographic filters," *Opt. Commun.*, vol. 30, pp. 163-165, Aug. 1979.
[32] R. J. Collier and K. S. Pennington, "Multicolor imaging from holograms formed on two-dimensional media," *Appl. Opt.*, vol. 6, pp. 1091-1095, June 1967.
[33] F. Krile, R. J. Marks, J. F. Walkup, and M. O. Hagler, "Holographic representation of space-variant systems using phase coded reference beams," *Appl. Opt.*, vol. 16, pp. 3131-3136, Dec. 1977.
[34] D. Gloge, "Weakly guiding fibers," *Appl. Opt.*, vol. 10, pp. 2252-2258, Oct. 1971.
[35] A. A. Friesem, Z. Rav-Noy, and S. Reich, "Photodielectric polymer for holographic recording," *Appl. Opt.*, vol. 16, pp. 427-432, Feb. 1977.
[36] R. J. Potter, "Transmission properties of optical fibers," *J. Opt. Soc. Am.*, vol. 51, pp. 1079-1089, Oct. 1961.
[37] W. Bronwer, *Matrix Methods in Optical Instrument Design.* New York: W. A. Benjamin, 1964.
[38] U. Levy, H. Kobrinsky, and A. A. Friesem, "Angular multiplexing for multichannel communication in a single fiber," *IEEE J. Quantum Electron.*, vol. QE-17, pp. 2215-2224, Nov. 1981.
[39] A. A. Friesem and U. Levy, "Direct pictorial transmission through optical fibers," in *Proc. Int. Conf. on Lasers '79.* McLean, VA: STS Press, 1980.
[40] D. Gloge, "Optical power flow in multimode fibers," *Bell Syst. Tech. J.*, vol. 51, pp. 1767-1783, 1972.
[41] L. Jeunhomme and J. P. Pocholle, "Angular dependence of the mode-coupling coefficients in a multimode optical fiber," *Electron. Lett.*, vol. 11, pp. 425-426, 1975.

Appendix B

Transmission of Two-dimensional Images through a Single Optical Fiber by Wavelength-Time Multiplexing

Published in Optics Letters, Vol.8, No.1, page 57, January 1983

Transmission of two-dimensional images through a single optical fiber by wavelength–time encoding

Anthony M. Tai and A. A. Friesem*

Radar and Optics Division, Environmental Research Institute of Michigan, P.O. Box 8618, Ann Arbor, Michigan 48107

Received July 2, 1982; revised manuscript received September 16, 1982

Serial transmission of image data through an optical fiber is inefficient in the utilization of the channel capacity of the fiber. Parallel image-transmission techniques, on the other hand, generally limit the transmission length to a few meters. A novel approach is introduced with which two-dimensional images can be efficiently transmitted through a single fiber at high speed. With this approach, images with space–bandwidth products greater than 2000 × 2000 can potentially be transmitted at a rate as high as 40 GHz.

Images are generally transmitted through optical fibers in one of three ways. The optical image may be sensed by an imaging detector and the data sent through an optical fiber by modulating the intensity of a light beam. Such a serial image-transmission scheme, however, does not utilize the channel capacity of the optical fiber efficiently. Moreover, the electronics in the imaging detector and modulator are highly susceptible to rf interference and radiation damage. For image transmission over a short distance, Selfoc fibers can be used. The image quality, however, deteriorates rapidly with distance. One may also transmit images through a coherent fiber bundle. The fiber bundle offers parallel image-transmission capability, but current manufacturing technology limits the transmission length to only a few meters.

To utilize the channel capacity of optical fibers more efficiently, wavelength encoding has been suggested as a means of transmitting images through a single fiber.[1,2] Such a scheme can provide the parallelism of a Selfoc fiber or a fiber bundle without the restriction on the fiber length. Implementing wavelength encoding–decoding is relatively simple for one-dimensional images. One may disperse the light emitted from a white-light point source into a line with a grating or a prism, projecting a different wavelength on each pixel of the object to encode the one-dimensional image. A second grating or prism is used to recombine the dispersed light, which is then coupled into the fiber. At the receiving end of the fiber, the transmitted light is dispersed again by a third grating, recreating the wavelength-encoded input image. Such a system utilizes the light energy efficiently, and there is no additional light loss beside the usual absorption, reflection, and coupling losses.

Extending the wavelength-encoding concept to two dimensions while maintaining the high efficiency is a difficult problem. In addition, using wavelength alone to encode two-dimensional images will severely restrict the space–bandwidth product of the images that can be transmitted. One may compromise by transmitting only one dimension in parallel. The most straightforward implementation is to utilize the one-dimensional system described earlier and simply translate the input object across the input plane.[3] Such an approach is simple but slow, negating many of the advantages offered by parallel transmission. Moreover, it is often impossible to translate the object to be imaged. In this Letter, we present an efficient optical system for the high-speed transmission of two-dimensional images by wavelength–time encoding.

First, let us assume that the input is in the form of a transparency. The image-transmission system is illustrated in Fig. 1. Three blazed reflection gratings are mounted on scanners that scan synchronously. The first grating disperses the light in the x direction, forming a line at the input plane, while the scanning causes the line to move across the input transparency along the y direction. The second grating recombines all the light, and the achromatic lens couples it into the fiber. We note that the elements are placed exactly one focal length apart such that the output forms a stationary white spot at the input of the fiber regardless of the positions of the synchronously scanning gratings. All the light emitted by the white-light point source (minus, of course, the light absorbed by the input

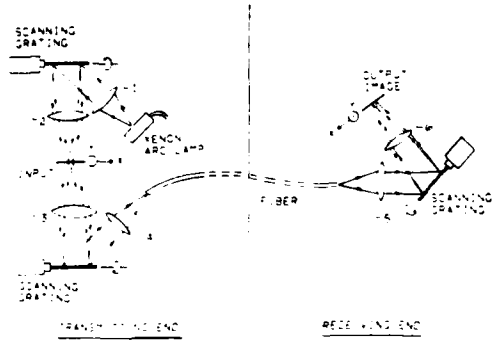

Fig. 1. Transmitting images on a transparency through a single fiber.

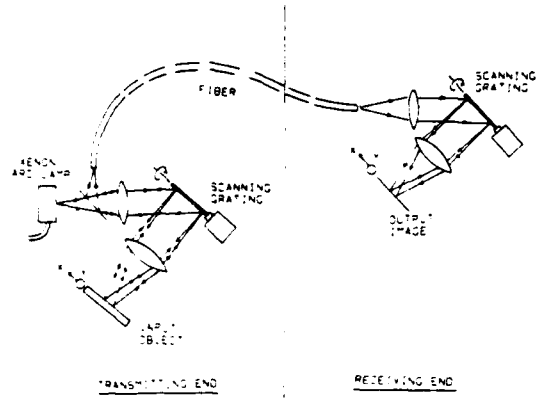

Fig. 2. Transmitting images of reflective objects through a single fiber with the illuminating source at the transmitting end.

transparency) is coupled into the fiber. This optical system can therefore achieve the same high efficiency as the simpler one-dimensional system.

The number of resolution elements that can be encoded by wavelength is determined by the fiber core diameter, the dispersiveness of the gratings, and the focal length of the lenses. For example, with a 1600-line/mm grating, visible light (4500 to 6500 Å) is dispersed into an angle of approximately 0.8 rad. If the fiber is multimode, the focused spot at the output plane corresponds to the image of the fiber core. Assuming that a one-to-one imaging geometry is used, the angle subtended by the output focused spot is then equal to D/F, where D is the diameter of the fiber core and F is the focal length of the lenses. Thus the number of resolution elements that can be encoded by wavelength is approximately $0.8F/D$. By using a 55-μm-diameter step-index fiber and 150-mm focal-length $f/1.2$ lenses, more than 2000 resolution elements can be encoded. By scanning in the y direction over the same angular range, images with 2000 × 2000 pixels can be transmitted. The scan rate of galvanometer scanners is limited to about 500 Hz (i.e., 1000 frames/sec). The data-transmission rate of the system is therefore equivalent to 4 GHz. The transmission rate can be further increased by using polygon rotating scanners. For example, when eight-facet scanners rotating at 75,000 rpm are used, the equivalent data-transmission rate will be 40 GHz. As a comparison, imaging detectors, such as charge-coupled-device arrays and vidicons, operate typically around 10 MHz and the frequency response of current light modulators is limited to about 2 GHz.

The transmission rate of the proposed system is not seriously affected by temporal dispersion in the fiber since the temporal rate of transmission (corresponding to the scanning along the y direction) is only 40 GHz/2000, or 20 MHz.

The optical system can also be used to image reflective objects, as shown in Fig. 2. In the reflection mode, the same grating is used to disperse and recombine the light, reducing the system length by half. Regardless of the position of the scanning grating, the light will be reflected back to form a white spot at the position of the light source. To couple the light into a fiber, a beam splitter is used to tap out the reflected light and direct it to the fiber.

We can take advantage of the fact that the light reflected off the object always refocuses back at the position of the source. In many applications, it is not possible to place a light source near the object to be imaged. One may transmit the illuminating light through the fiber from the receiving end. The light is dispersed at the transmitting side and used to encode the object. The light reflected by the object is recombined and coupled back into the same fiber, as shown in Fig. 3. The returned light is redispersed at the output to form the object image. Placing the light source at the receiving end could result in strong reflections off the fiber–air interfaces that sharply reduce the output image contrast. To eliminate such reflections, the fiber is bonded to a thick (1.25-cm) beam splitter at the receiving end and to a glass window at the transmitting end with index-matching optical epoxy. With this arrangement, the reflections from the interfaces are directed away from the output plane.

To transmit the image of a distant object, it is not possible to synchronize the scanning motors by direct hookup. One possible approach that can be employed to synchronize the scanning motors is to place a small mirror at the object plane. The mirror will reflect strongly, creating a reference that can be used for synchronizing the scanners. The strong return may be used as a trigger for the scanner at the output, or it may be used as a point reference for adjusting the scanner frequency and phase.

A better approach is to make use of the second-order diffraction of the encoding grating to achieve self-referencing. By choosing the appropriate diffraction angle and geometry, one can make the second-order diffraction propagate back to the source, as illustrated in Fig. 3. This creates a dispersed line that scans across the fiber as the grating rotates and produces a single bright spot at the output image that can be used to synchronize the scanner at the receiving end.

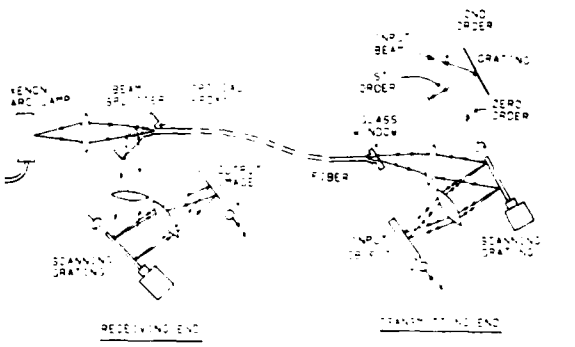

Fig. 3. Transmitting images of reflective objects through a single fiber with the illuminating source at the receiving end.

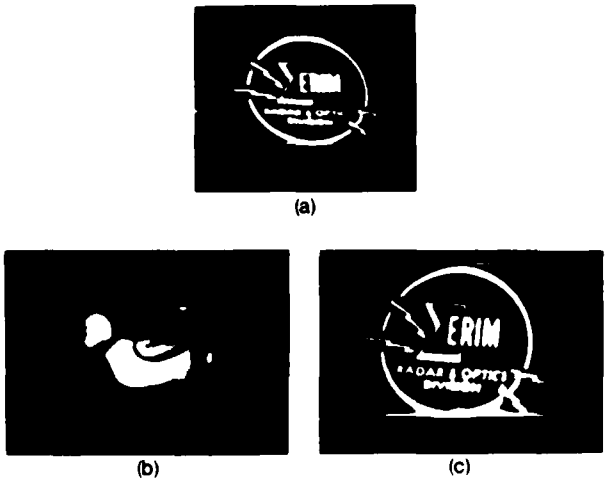

Fig. 4. Images transmitted through a single fiber. (a) Image of a transparency transmitted through a fiber with a 600-μm-diameter core. (b) Image of a diffuse three-dimensional object transmitted through a fiber with a 600-μm-diameter core. (c) Image of a transparency transmitted through a fiber with a 200-μm-diameter core.

The image brightness is affected by the numerical aperture, the core size, and the length of the fiber. It is also determined by the scan rate and observation time. In order to optimize the system efficiency, lenses 1, 4, and 5 of Fig. 1 should be matched to the numerical aperture of the fiber ($f/2$ lenses for a fiber with N.A. = 0.25), and lenses 2, 3, and 6 should be matched to the dispersiveness of the grating ($f/1.2$ lenses for 0.8 rad of dispersion).

A 75-W xenon-arc lamp was used in our experiments. For an all-white input (transmittance = 1), the intensities of the image transmitted through 25 m of fibers (N.A. = 0.3, attenuation = −20 dB/km) with core diameters of 600 and 200 μm using the system depicted in Fig. 1 were measured to be about 1 and 0.3 mW/cm^2, respectively. The measurements were made with the scanners kept stationary. Two-dimensional images were transmitted by scanning the dispersed light line across the input image. Thus each resolution spot at the output appeared for only $1/N$ of the frame time, where N is the number of resolution spots along the scanned direction. Since the frame time (2 msec) was much shorter than the integration time of the eye, the observed image brightness was equal to the image intensity multiplied by the duty cycle, $1/N$. The observed brightness of the images transmitted through the 600- and 200-μm fibers was therefore about 10 and 1 μm/cm^2, respectively.

We stated earlier that the system is capable of transmitting images at a rate as high as 40 GHz. However, to be able to take advantage of this high transmission rate, one must have the means available to receive the data. One possibility is to record each individual frame of the transmitted image on film with a setup similar to a high-speed camera. Since the exposure time will be short, an image intensifier will be necessary to increase the output-image illuminance. This power-budget problem will ultimately place a limit on the transmission rate and/or the transmission length.

In our experiments, we first used a 25-m long silica fiber with a 600-μm-diameter core and a N.A. of 0.3. In Fig. 4(a) we show the transmitted image of a transparency made using the system depicted in Fig. 1; in Fig. 4(b) we show the image of a three-dimensional diffused object transmitted with the system illustrated in Fig. 2. The bright spot that appears at the feet of the toy duck is the point reference created by the second-order diffraction.

The spectral range occupied by the image field is 5000 to 6000 Å. Thus the space–bandwidth product of the image transmitted is about 100 × 100. This rather moderate image resolution is due mainly to the large fiber-core size. The space–bandwidth products of the images transmitted can be significantly increased by using fibers with smaller core diameters. For example, in Fig. 4(c) we show the result obtained with a fiber having a 200-μm-diameter core. The space–bandwidth product of the image field is approximately 300 × 300. The images are recorded by pointing the camera directly at the output grating. The images were bright enough to be seen in room light provided that the output optics were properly shielded.

The proposed optical system for transmitting two-dimensional images through a single fiber is expected to be useful for the following applications: (1) Real-time remote observation of rapidly changing or short-lived events. By using a rotating polygon scanner, more than 10,000 frames can be transmitted per second. Just as important, each line is encoded and transmitted in less than 50 nsec. Thus objects moving slower than 1 pixel/50 nsec (1.1 km/sec for a 55-μm pixel) can be resolved clearly, albeit with some geometric distortion. (2) Remote observation of events in a hostile environment. The electronics in optical modulators and imaging detectors are prone to rf interference and radiation damage. The electronics required in the proposed system is a low-frequency driving circuit for the synchronous motor. It is generally much more resistant to interference or damage.

We are grateful to Y. Silberberg for many valuable discussions and to David Fienup for his contribution of the toy duck. This research was supported by U.S. Army Research Office contract DAAG-81-K-0129.

* On sabbatical from the Weizmann Institute of Science, P.O. Box 26, Rehovot, Israel, during 1981–1982.

References

1. A. A. Friesem and U. Levy, Opt. Lett. **2**, 133 (1978).
2. A. A. Friesem and U. Levy, in *Proceedings of the International Conference on Lasers 79* (STS, McLean, Va., 1980), p. 425.
3. S. Case, Progress Rep. to U.S. Army Research Office, contract DAAG29-81-K-0033 (1982).

Appendix C

Two-dimensional Image Transmission through a Single Optical Fiber by Wavelength-Time Multiplexing

Published in Applied Optics, Vol.23, page 3826, December 1983

Reprinted from **Applied Optics**, Vol. 22, page 3826, December 1, 1983

Two-dimensional image transmission through a single optical fiber by wavelength-time multiplexing

Anthony M. Tai

Serial transmission of image data through an optical fiber is inefficient in the utilization of the channel capacity of the fiber. Parallel image transmission techniques, on the other hand, generally limit the transmission length to a few meters. A novel approach is introduced with which 2-D image data can be transmitted efficiently at high speed over a single optical fiber using wavelength–time multiplexing. Several system configurations designed for different types of input are presented.

I. Introduction

Images are generally transmitted through optical fibers in one of three ways. First, the optical image may be sensed by an imaging detector and the data sent through an optical fiber a pixel at a time by modulating the intensity of a light beam. Such a serial image transmission scheme, however, does not utilize the channel capacity of the optical fiber efficiently. Moreover, the electronics in the imaging detector and modulator are highly susceptible to rf interference and radiation damage. Second, images can be transmitted in parallel over a short distance using Selfoc fibers. The image quality, however, deteriorates rapidly with distance. Finally, one may transmit images through a coherent fiber bundle. The fiber bundle offers parallel image-transmission capability, but current manufacturing technology limits the transmission length to only a few meters.

To utilize more fully the channel capacity of optical fibers, wavelength encoding has been suggested as a means of transmitting images through a single fiber.[1-7] Such a scheme can provide the parallelism of a Selfoc fiber or a fiber bundle without the restriction on the fiber length. Implementing wavelength encoding–decoding is relatively simple for 1-D images. One may disperse the light emitted from a white-light point source into a line with a grating or a prism, projecting a different wavelength on each pixel of the object to encode the 1-D image. A second grating or prism is used to recombine the dispersed light, which is then coupled into the fiber. At the receiving end of the fiber, the transmitted light is dispersed again by a third grating, recreating the wavelength-encoded input image. Such a system utilizes the light energy efficiently, and there is no additional light loss beside the usual absorption, reflection, and coupling losses.

Extending the wavelength-encoding concept to two dimensions while maintaining high efficiency is a difficult problem. In addition, using wavelength alone to encode 2-D images will severely restrict the space–bandwidth product of the images that can be transmitted. One may compromise by transmitting only one dimension in parallel. The most straightforward implementation is to utilize the 1-D system described earlier and simply translate the input object across the input plane.[6,7] Such an approach is simple but slow, negating the main advantage offered by parallel transmission. Moreover, it is often impossible to translate the object to be imaged. In this paper, we present an efficient system approach for the high-speed transmission of 2-D images by wavelength-time encoding.[8,9]

II. Transmissive Input

First, let us assume that the input is in the form of a transparency. The image transmission system is illustrated in Fig. 1. Three blazed reflection gratings are mounted on scanners that scan synchronously. The first grating disperses the light in the x direction, forming a line at the input plane, while the scanning causes the line to move across the input transparency along the y direction. The second grating recombines all the light, and the achromatic lens couples it into the fiber. We note that the elements are placed exactly one focal length apart so that the output forms a stationary white spot at the input of the fiber regardless of the

The author is with Environmental Research Institute of Michigan, Infrared & Optics Division, P.O. Box 8618, Ann Arbor, Michigan 48107.

Received 30 June 1983.
0003-6935/83/233826-07$01.00/0.

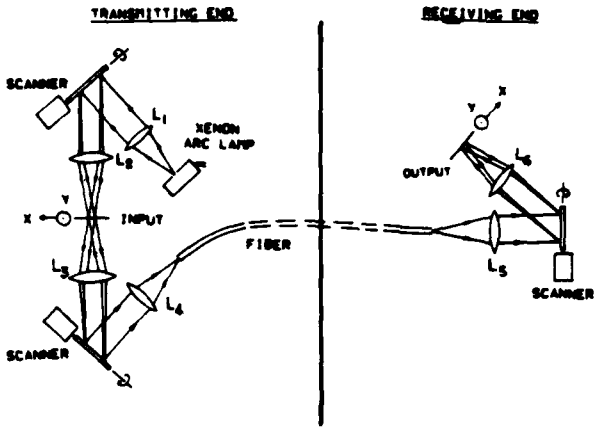

Fig. 1. System for transmitting images of a transmissive object through a single optical fiber.

positions of the synchronously scanning gratings. All the light emitted by the white-light point source (minus, of course, the light absorbed by the input transparency) is coupled into the fiber. This optical system can, therefore, achieve the same high efficiency as the simpler 1-D system.

The dispersiveness of a blazed grating is dependent on the spatial frequency of the grating, the blaze angle, and the angle of the incident beam. With the geometry shown in Fig. 2(a), the angle of the diffracted beam is equal to

$$\theta_0 = \sin^{-1}(g\lambda - \sin\theta_i), \tag{1}$$

where g is the grating frequency, λ is the wavelength, and θ_i is the incident beam angle. (For a given blaze angle, there are only two possible incident angles that satisfy the condition for high diffraction efficiency.) Taking the derivative with respect to λ, we obtain the dispersion of the grating:

$$\frac{d\theta_0}{d\lambda} = \frac{g}{[1 - (g\lambda - \sin\theta_i)^2]^{1/2}}. \tag{2}$$

As an example, suppose that we have a blazed grating with g = 1500 grooves/mm and a blaze angle of 28°, and we want to use it to disperse a beam with a wide spectral bandwidth centering at 550 nm. The beam can be launched onto the grating normally or at an angle of 56° as shown in Figs. 2(b) and (c). Launching the beam normally results in a dispersion of

$$\frac{d\theta_0}{d\lambda} = \frac{g}{[1 - (g\lambda)^2]^{1/2}} = 2.65 \times 10^6 \text{ rad/m},$$

while launching the beam at an angle of 56° produces a dispersion of

$$\frac{d\theta_0}{d\lambda} = \frac{g}{[1 - (g\lambda - \sin(56°))^2]^{1/2}} = 1.5 \times 10^6 \text{ rad/m}.$$

Thus we see that launching the incident beam normally onto the grating produces a substantially higher dispersion. It is for this reason that we choose such a geometry in implementing the image transmission system illustrated earlier in Fig. 1. An additional advantage

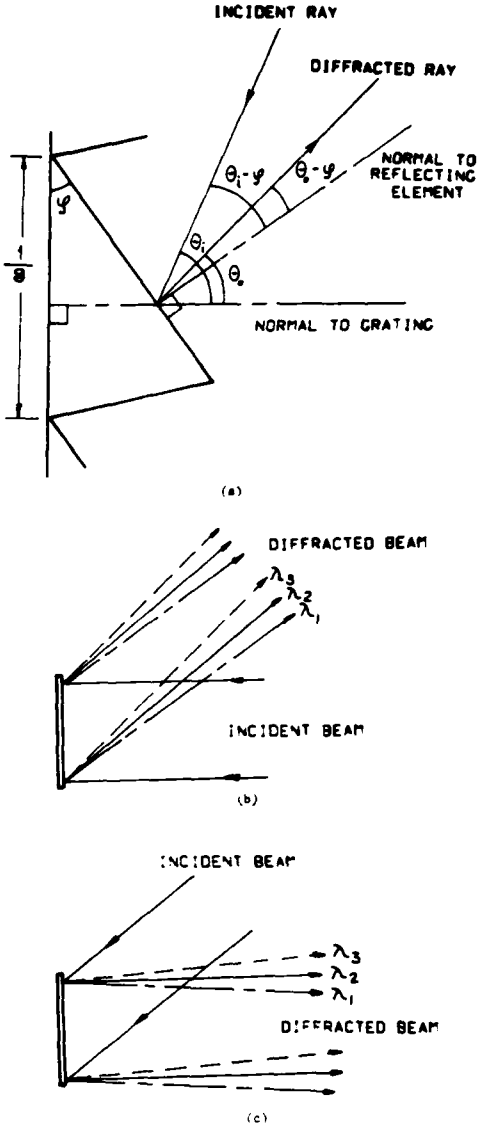

Fig. 2. Diffraction by a blazed grating: (a) geometry of blazed grating; (b) normal incident beam; (c) oblique incident beam.

in using a normal incident beam is that the width of the diffracted beam is compressed instead of expanded as with the case of an oblique incident beam. The demand on the focusing lens is thus reduced.

III. Space-Bandwidth Product and Image Brightness

The number of resolution elements that can be encoded is determined by the fiber core diameter, the dispersion of the gratings, and the focal length of the lenses. For example, with a grating with g grooves/mm, a light beam whose spectral bandwidth extends from λ_1 to λ_2 is dispersed into an angle

$$\Delta\theta = \sin^{-1}(g\lambda_2) - \sin^{-1}(g\lambda_1). \tag{3}$$

Focusing with a lens with focal length f, the dispersion produces a line $2f \tan(\Delta\theta/2)$ long. If the fiber is mul-

timode, the focused spot at the output plane corresponds to the image of the fiber core. Assuming that all the lenses in Fig. 1 have the same focal length, we have a one-to-one imaging geometry, and the number of resolvable spots is equal to

$$N = 2f \tan(\Delta\theta/2)/D, \tag{4}$$

where D is the diameter of the fiber core. As an example, if g = 1500 grooves/mm, f = 150 mm, D = 55 μm, λ_1 = 450 nm, and λ_2 = 650 nm, then $\Delta\theta$ = 0.6 rad and N = 1704. By scanning in the y direction over the same angular range, images with 1700 × 1700 pixels can be transmitted.

The scan rate of galvanometer scanners is limited to ~500 Hz (i.e., 1000 frames/sec). The data transmission rate of the system is, therefore, equivalent to 2.89 GHz. The transmission rate can be further increased by using polygon rotating scanners. For example, when eight-facet scanners rotating at 75,000 rpm are used, the equivalent data-transmission rate will be 28.9 GHz. As a comparison, imaging detectors, such as charge-coupled-device arrays and vidicons, operate typically ~10 MHz, and the frequency response of current light modulators is limited to ~2 GHz.

The transmission rate of the proposed system is not seriously affected by temporal dispersion in the fiber since the temporal rate of transmission (corresponding to the scanning along the y direction) is only 28.9 GHz/1700 or 17 MHz.

The image brightness is affected by the numerical aperture, core size, and length of the fiber. It is also determined by the scan rate and observation time. To optimize the system efficiency, lenses 1, 4, and 5 of Fig. 1 should be matched to the numerical aperture of the fiber (f/2 lens for a fiber with N.A. = 0.25), and lenses 2, 3, and 6 should be matched to the dispersiveness of the gratings (lenses with f/No. smaller than f/1.6 for 0.6 rad of dispersion).

Light sources used for illumination such as arc lamps are small but nevertheless extended sources. What appears at the input of the fiber is essentially the image of the source. In general, the core diameter of the fiber is much smaller than the source image, and the amount of light coupled is proportional to D^2, where D is the diameter of the fiber core. The space–bandwidth product of the image transmitted on the other hand is equal to N^2, which is proportional to $1/D^2$. Thus there is a direct trade-off between the efficiency and space–bandwidth product of the image transmission system.

The amount of light that can be coupled into a fiber is also determined by the cone angle of acceptance or the numerical aperture of the fiber. The numerical aperture of a fiber is equal to[10]

$$\text{N.A.} = \frac{n_{\text{core}}}{n_{\text{air}}} \cdot \cos\left[\sin^{-1}\left(\frac{n_{\text{cladding}}}{n_{\text{core}}}\right)\right] = (n_{\text{core}}^2 - n_{\text{cladding}}^2)^{1/2}/n_{\text{air}}. \tag{5}$$

Thus system efficiency is maximized by using a fiber with a large differential between the refractive indices of the core and the cladding. Such a fiber, however, also tends to exhibit strong modal dispersion which may limit the transmission rate. Fortunately, due to the parallelism of the transmission system where N pixels are transmitted simultaneously, the temporal rate is fairly low even if the overall system transmission rate is extremely high (17 MHz vs 28.9 GHz in our earlier example).

To take full advantage of the high transmission rate this transmission approach offers, a means must be available to receive the data. One possibility is to record each individual frame of the transmitted image on film using an arrangement similar to a high-speed camera. The equivalent exposure time is very short, and an image intensifier may be necessary to increase the output image illuminance. This power budget problem may ultimately impose a practical limit on the transmission rate and/or transmission length.

The amount of energy E that is available for each pixel of image data is proportional to

$$E \propto \frac{1}{N^2 T} \propto \frac{D^2}{T}, \tag{6}$$

where T is the frame time. To increase E, one can either increase the diameter of the fiber core D or decrease T by slowing down the scanning mechanism. The transmission rate, on the other hand, is equal to

$$R = N^2 T \propto \frac{T}{D^2}. \tag{7}$$

Thus

$$E \propto (1/R). \tag{8}$$

To increase the amount of light available for image data will require a proportional reduction in the transmission rate.

In our experiments to demonstrate the image transmission system, a 75-W xenon-arc lamp was used as the illuminating source. For an all-white input (transmission = 1), the intensities of the image transmitted through 25 m of fibers (N.A. = 0.3, attenuation = −20 dB/km) with core diameters of 600 and 200 μm using the system depicted in Fig. 1 were measured to be ~1 and 0.3 mW/cm^2, respectively. The measurements were made with the scanners kept stationary. Two-dimensional images were transmitted by scanning the dispersed light line across the input image. Thus each resolution spot at the output appeared for only $1/N$ of the frame time, where N is the number of resolution spots along the scanned direction. Since the frame time (2 msec) was much shorter than the integration time of the eye, the observed image brightness was equal to the image intensity multiplied by the duty cycle $1/N$. The observed brightness of the images transmitted through the 600- and 200-μm fibers was, therefore, ~10 and 1 μW/cm^2, respectively. We note that at such a brightness level and frame time, individual frames may be recorded with a moderately fast (400 ASA) photographic film.

In Fig. 3(a) we show the transmitted image of a transparency obtained by using the system depicted in Fig. 1. The space–bandwidth product of the images

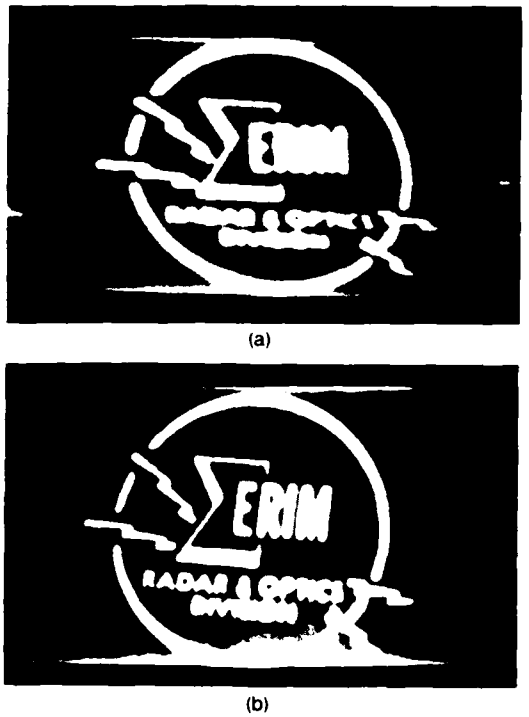

Fig. 3. Images of a transmissive object transmitted through a single fiber: (a) image of a transparency transmitted through a fiber with a 600-μm diam core; (b) image of a transparency transmitted through a fiber with a 200-μm diam core.

transmitted is $\sim 100 \times 100$. This rather moderate image resolution is due mainly to the large fiber-core size. The space–bandwidth products of the images transmitted can be significantly increased by using fibers with smaller core diameters. For example, in Fig. 3(b) we show the result obtained with a fiber having a 200-μm diam core. The space–bandwidth product of the image field is $\sim 300 \times 300$. The images are recorded by pointing the camera directly at the output grating.

The images are quite bright, especially when observed by looking directly into the output grating. By shielding the output optics to prevent spurious light from being diffracted into the eye, the image can easily be observed in normal room light.

IV. Reflective Inputs

The optical system can also be used to image reflective objects, as shown in Fig. 4. In the reflection mode, the same grating is used to disperse and recombine the light, reducing the system length by half. Regardless of the position of the scanning grating, the light will be reflected back to form a white spot at the position of the light source. To couple the light into a fiber, a beam splitter is used to tap out the reflected light and direct it to the fiber.

To transmit the image of a distant object, it is not possible to synchronize the scanning motors by direct hookup. One possible approach that can be employed to synchronize the scanning motors is to place a small mirror at the object plane. The mirror will reflect

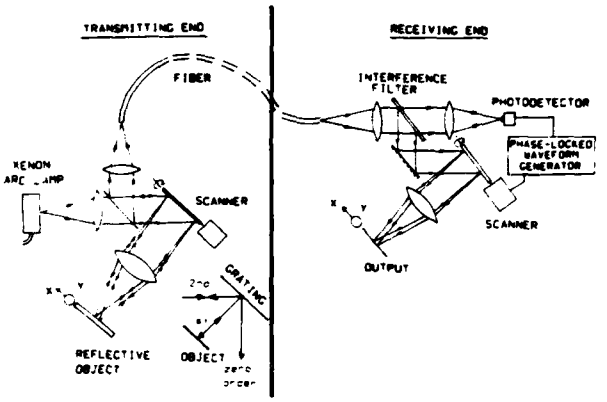

Fig. 4. System for transmitting a reflective object using the second-order diffraction to generate the referencing signal.

strongly, creating a reference that can be used for synchronizing the scanners. The strong return may be used as a trigger for the scanner at the output, or it may be used as a point reference for adjusting the scanner frequency and phase.

A much better approach, however, is to create a self-referencing optical signal that can be used for the synchronization of the scanners. A novel method of generating such a signal is to utilize the second-order diffraction of the encoding grating. By launching the wideband input beam onto the grating normally and choosing an appropriate grating geometry, the second-order diffraction can be made to propagate directly back toward the source as illustrated in Fig. 4. This creates a color dispersed line that is scanned across the fiber as the grating rotates and produces a single bright spot at the decoded output. The location of the reference spot can be adjusted by changing the geometry of the optics. A color is chosen for the reference light spot so that it appears at the edge of the image field. Since the image is color-encoded, this will allow the reference spot and the target image to be separated using a spectral filter.

In our experiment, an interference filter was used as a beam splitter which transmitted the color of the reference spot and reflected all other wavelengths. The reference signal was detected by a photodiode, and the output pulses were used to trigger a signal generator. In Fig. 5(a), we show the position output of the scanner controller at the transmitting end together with the output of the photodetector at the receiving side. We see that a synchronous trigger pulse was generated every time the galvanometer scanned through one cycle. The output of the phase-locked signal generator was then used to drive the scanner at the receiving end. In Fig. 5(b), we show the position outputs of the two scanner controllers. The scanners were well synchronized.

We emphasize that, using this technique, the image transmission and synchronization were performed entirely by optical means with only a single optical fiber connecting the transmitting and receiving ends. In Fig. 6, we show the image of a diffuse reflective object transmitted with the system depicted in Fig. 4. The

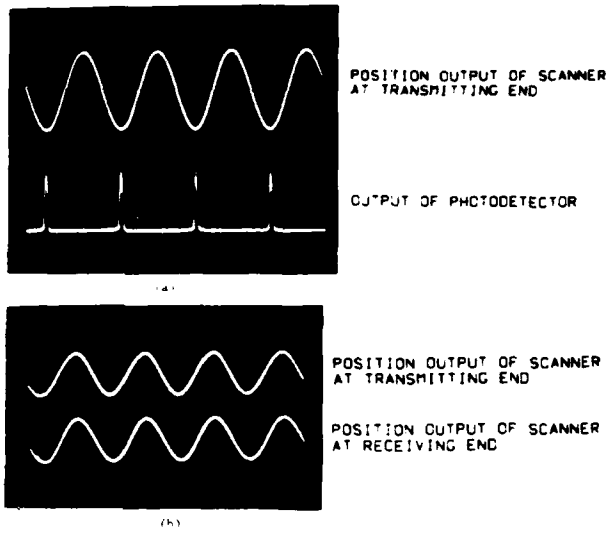

Fig. 5. Synchronization of the scanners at the transmitting and receiving ends: (a) oscilloscope traces of the position output of the scanner at the transmitting end and the output of the photodetector at the receiving end; (b) oscilloscope traces of the position outputs of the scanners at the transmitting and receiving ends.

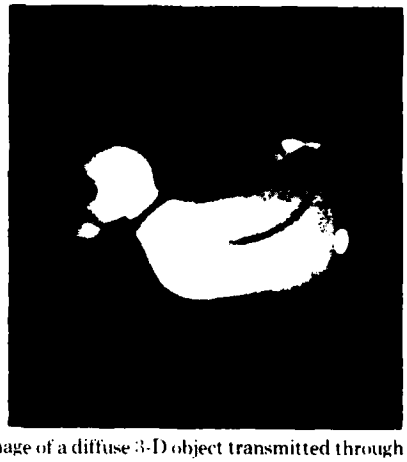

Fig. 6. Image of a diffuse 3-D object transmitted through a fiber with a 600-μm diam core.

fiber has a 600-μm diam core, and the space–bandwidth product of the image is $\sim 100 \times 100$. Since the object was diffuse, the transmitted image was dimmer than that obtained with a transparency as the input. Nevertheless, the image was still bright enough to be observed by looking directly into the output grating.

We can also take advantage of the fact that the light reflected off the object always refocuses back at the position of the source. In many applications, it is not possible to place a light source near the object to be imaged. One may transmit the illuminating light through the fiber from the receiving end. The light is dispersed at the transmitting side and used to encode the object. The light reflected by the object is recombined and coupled back into the same fiber, as shown in Fig. 7. The returned light is redispersed at the output to form the object image. Placing the light source at the receiving end could result in strong reflections off the fiber–air interfaces that sharply reduce the output image contrast. To eliminate such reflections, the fiber is bonded to a thick (1.25-cm) beam splitter at the receiving end and to a glass window at the transmitting end with index-matching optical epoxy. With this arrangement, the reflections from the interfaces are directed away from the output plane.

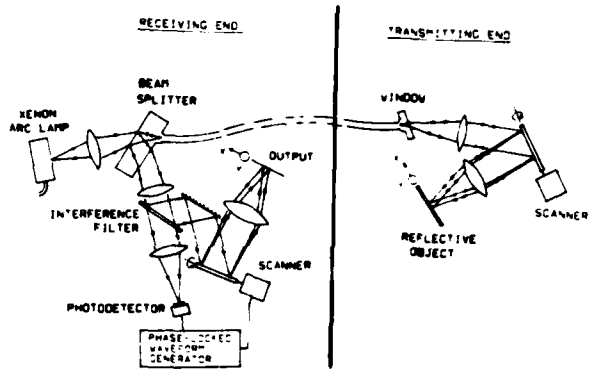

Fig. 7. Transmitting images of a reflective object through a single fiber with the illuminating source at the receiving end.

V. Self-emissive or Naturally Illuminated Inputs

With the previously described systems, the object is actively illuminated with a wavelength-encoded beam. The system can also be used to transmit images of self-emissive objects by simply removing the light source and replacing the beam splitter in the system depicted in Fig. 4 with a mirror. However, the system is much less efficient when working in this mode. Assuming that the object is emitting white light, the amount of light energy transmitted is only $1/N$ of the total light energy received by the lens where N is the number of pixels encoded by wavelength. Nevertheless, if the object is sufficiently bright, the system can be used to transmit passively the object image. For example, in Fig. 8(a), we show the transmitted image of the coil filament of a 25-W incandescent lamp.

A more efficient technique of transmitting images of self-emissive or naturally illuminated objects is to first

Fig. 8. Images of self-emissive and passively illuminated objects transmitted through a single fiber: (a) the coil filament of an incandescent lamp; (b) a human hand illuminated with a 40-W incandescent light bulb.

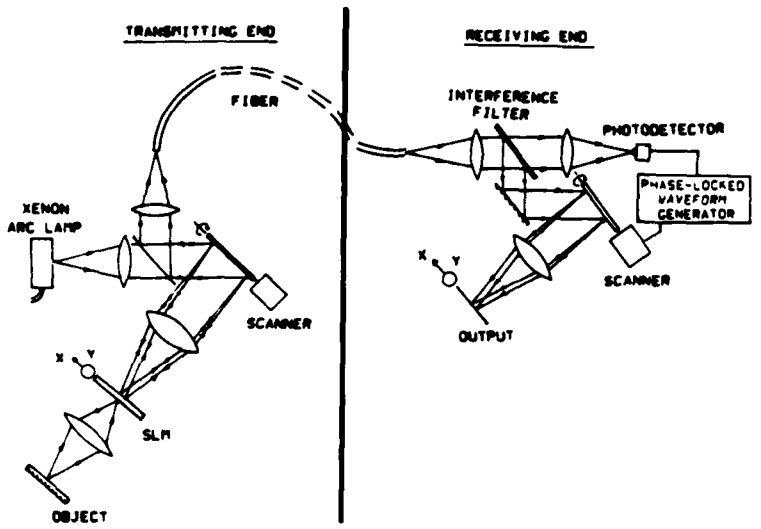

Fig. 9. System for transmitting images of self-emissive or passively illuminated object using a SLM to create a secondary image.

create a secondary image which can be actively read out and transmitted. For example, the object can be imaged onto a spatial light modulation (SLM) which is read out by the wavelength-encoded beam as shown in Fig. 9. The SLM provides a new input whose image can be efficiently transmitted through the optical fiber. The $1/N$ factor is avoided, and the system efficiency is greatly enhanced. However, the response time of the SLM will limit the system transmission rate. Using a SLM with a cycling rate of 30 frames/sec to transmit images with 1700×1700 pixels, the effective transmission rate is only 86.7 MHz. Nevertheless, the system still offers the advantages of transmitting images with a large space–bandwidth product at potentially lower cost.

The space–bandwidth products of images transmitted by conventional techniques are limited by the imaging detector. For example, a typical CCD detector array is composed of 512×512 or fewer detector elements. A mosaic of detector arrays is used when larger space–bandwidth product is desired. The cost of such a system can be exceedingly high. A SLM, on the other hand, can provide a space–bandwidth product of 2000×2000 or better. Since the transmission rate is relatively slow, power budget is much less a problem, and the optical system can also be made to transmit images with 2000×2000 pixels or more by using a fiber with a smaller fiber core or lenses with longer focal lengths [see Eq. (4)].

To demonstrate the system approach, we performed an experiment using a Hughes liquid crystal light valve as the SLM. In Fig. 8(b), we show the transmitted image of a human hand which was illuminated by a single 40-W incandescent light bulb. The light valve is capable of resolving 30 lines/mm over a 45-mm diam working aperture. This would provide a space–bandwidth product equivalent to 1200×1200 pixels. However, a fiber with a 200-mm diam core was used in the experiment, and the space–bandwidth product of the transmitted image field was only $\sim 250 \times 250$. Moreover, the use of a liquid crystal light valve could hardly qualify the system as being low cost. We are currently developing at ERIM a low-cost high-resolution reflective elastomeric light modulator which may make an image transmission system as depicted in Fig. 9 very competitive for high-resolution image transmission applications.

VI. Summary

High-speed image transmission demands a very high data transmission rate. Optical fibers offer the necessary channel capacity to satisfy the demand. However, conventional serial transmission techniques are not very efficient in the utilization of the available channel capacity. With the wavelength–time multiplexing approach presented in this paper, a large number of pixels (corresponding to the number of resolution spots along one dimension) are transmitted simultaneously in parallel through the single optical fiber. The channel capacity of the fiber is, therefore, much more efficiently utilized. In addition, conventional optical communication schemes require four signal conversion steps. Typically, the original optical input is converted into an electrical signal (via an imaging detector), then into an optical signal (via a laser diode) and to an electrical signal again (via a photodetector), and finally back to an optical signal (via a CRT). The proposed imaging transmission approach offers a means to eliminate all these conversion steps, transmitting the optical input directly through the optical fiber and reproducing the image at the receiving end.

The proposed optical system for transmitting 2-D images through a single fiber is expected to be useful for the following applications: (1) Real-time remote observation of rapidly changing or short-lived events. By using a rotating polygon scanner, more than 10,000 frames can be transmitted per second. Just as important, each line is encoded and transmitted in <60 nsec. Thus objects moving slower than 1 pixel/60 nsec (0.9 km/sec for a 55-μm pixel) can be resolved clearly, albeit

with some geometric distortion. (2) Remote observation of events in a hostile environment. The electronics in optical modulators and imaging detectors are prone to rf interference and radiation damage. The electronics required in the proposed system is a low-frequency driving circuit for the synchronous motor. It is generally much more resistant to interference or damage. (3) Transmission of high-resolution images. The space–bandwidth product of the image that can be transmitted conventionally is limited by the imaging detector. To transmit images with much more than 512 × 512 pixels requires costly mosaic arrays. The proposed system approach offers a potentially more economical means of detecting and transmitting high-resolution imageries.

The author gratefully acknowledges A. Friesem and Y. Silberberg for many valuable discussions, D. Fienup for his contribution of the toy duck, and J. Cederquist for lending his hand in the experiment. The research was supported by U.S. Army Research Office contract DAAG-81-K-0129.

References

1. A. A. Friesem and U. Levy, Opt. Lett. **2**, 133 (1978).
2. A. A. Friesem and U. Levy, in *Proceedings, International Conference on Lasers 79* (STS, McLean, Va., 1980), p. 425.
3. J. D. Armitage *et al.*, Jpn. J. Appl. Phys. **4**, 273 (1965).
4. H. O. Bartelt, Opt. Commun. **27**, 365 (1978).
5. H. O. Bartelt, Opt. Commun. **28**, 45 (1979).
6. B. Adams and S. K. Case, Appl. Opt. **22**, 2026 (1983).
7. D. E. Husley and S. K. Case, Appl. Opt. **22**, 2029 (1983).
8. A. A. Friesem, U. Levy, and Y. Silberberg, Proc. IEEE **77**, 208 (1983).
9. A. M. Tai and A. A. Friesem, Opt. Lett. **8**, 57 (1983).
10. D. B. Keck and R. E. Love, in *Applied Optics and Optical Engineering, Vol. 6*, R. Kingslake and B. J. Thompson, Eds. (Academic, New York, 1980), Chap. 11.

Appendix D

Computer-Generated Holograms for Geometric Transformation

Published in Applied Optics, Vol. 23, page 3099, September 1984.

Reprinted from Applied Optics, Vol. 23, page 3099, September 15, 1984

Computer-generated holograms for geometric transformations

Jack Cederquist and Anthony M. Tai

Theory and experiments in the area of computer-generated holograms for geometric transformations are presented. Geometric transform holograms are divided into two categories: (1) those which have a continuous fringe structure, and (2) those which consist of a set of discrete subholograms. Criteria for the realizability of a continuous geometric transform hologram are described. Examples of both types of hologram are developed to map rings of different radii to a linear sequence of points. They allow the replacement of a ring detector by a linear detector array without loss of signal energy and can be applied to optical spectrum analysis and angle-wavelength multiplexing for data transmission through optical fibers.

I. Introduction

The use of computer-generated holograms (CGHs) to perform geometric transformations was first investigated by Bryngdahl[1,2] nearly ten years ago. There continues to be much interest in and many applications for optical geometric transformations. Recent work includes holographic elements for the redistribution of illumination,[3] deformable mirrors for distortion compensation,[4] and anamorphic optics for map transformation.[5] The current capability of producing CGHs having large space–bandwidth product using electron-beam lithography, high-quality CRT displays imaged onto a translatable photographic plate, or high-resolution rotating drum laser film recorders should stimulate further research.

Applications of a ring-to-point geometric transformation are described in Sec. II. In Sec. III, the general optical system configuration that utilizes CGHs to perform geometric transformations is analyzed. Two types of CGH are defined. Experiments involving each type of CGH are discussed in Sec. IV.

II. Applications for Ring-to-Point Transform CGH

A CGH which transforms rings to points with the radius of the ring corresponding to the position of the point along a line (see Fig. 1) has useful applications in the areas of optical fiber data transmission, detection of a spatial frequency spectrum, and confocal Fabry-Perot spectrum analysis.

A. Angle-Wavelength Multiplexing in Optical Fibers

In angle multiplexing for optical fiber communication, narrow input beams at a range of angles are coupled into a multimode step-index fiber.[6] At the output, each input beam will be converted into a cone of illumination (see Fig. 2). If the output light from all the beams is collimated with a lens, a ring-to-point transform CGH and lens combinnation can be used to collect the light in each ring and bring it to focus on a detector (see Fig. 1). The light efficiency of the demultiplexing process can, therefore, be very high.

In wavelength multiplexing,[7] beams of different wavelengths are coupled into the fiber. At the output the light is dispersed by a grating and demultiplexed into separate channels. Angle and wavelength multiplexing can be implemented together using a rings-to-points geometric transform hologram fabricated with a high carrier frequency. One possible configuration is illustrated in Fig. 3. The input is a 2-D array of sources such as LEDs or laser diodes. The light sources along the x direction emit the same wavelength, and the wavelengths for the different rows of sources are chosen so that they are recombined by the diffraction grating. All the light is coupled into the fiber with the light emanating from each column of light sources entering the fiber at a different entrance angle. At the output, the geometric transform CGH and the lenses redistribute the light from different cone angles into a linear array of points in the x direction, while the carrier frequency disperses the light in the y direction. The fiber output is thus demultiplexed and reformatted into a 2-D array of points which are received by a detector array.

The authors are with Environmental Research Institute of Michigan, P.O. Box 8618, Ann Arbor, Michigan 48107.
Received 3 February 1984.
0003-6935/84/183099-06$02.00/0.

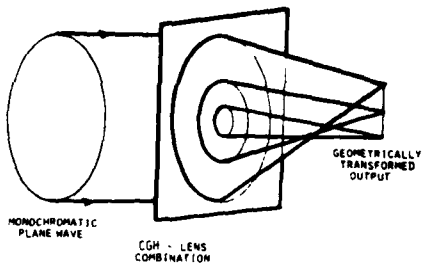

Fig. 1. Ring-to-point geometric transformation.

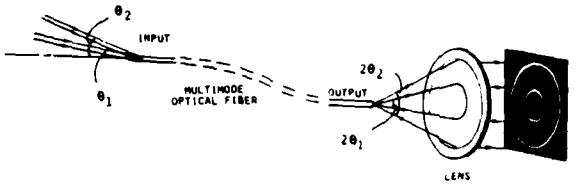

Fig. 2. Angle multiplexing in optical fibers.

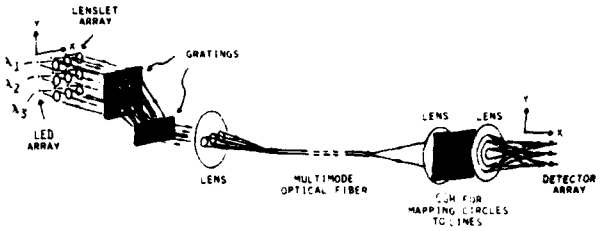

Fig. 3. Angle-wavelength multiplexing for data transmission through optical fibers.

B. Spatial Frequency Spectrum Detection

One method for detecting spatial-frequency spectra is by means of ring and wedge-shaped photodetector elements to provide integrated spatial frequency and orientation information. They are used in automatic inspection systems for quality control. Their drawback is that ring-wedge detectors are expensive, and, because of the large area of each detector element, the response time is slow. The ring-to-point CGH can be used to focus the light from a series of concentric rings onto a series of small area detector elements, thus replacing the ring detector. Linear detector arrays are relatively inexpensive and have much faster response. A wedge-to-point CGH could similarly be made to replace the wedge detector.

C. Confocal Fabry-Perot Spectrum Analyzer

Defocused confocal Fabry-Perot spectrum analyzers produce an output which is a series of concentric rings, one ring for each wavelength present in the input light. Detection of the spectrum is usually by piezoelectric scanning of the mirror separation and use of a single on-axis photodetector. An alternate is to use a CGH and parallel readout of a linear array of detectors. Light efficiency is higher, no mechanical scanning is required, and parallel analysis of the entire spectrum is achieved.

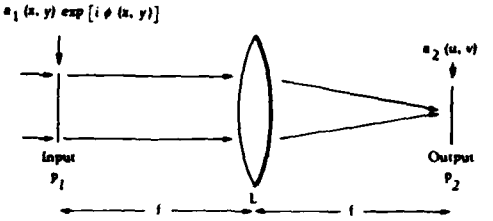

Fig. 4. One hologram system for geometric transformation.

III. Theory

In this section, an optical system used for geometric transformations is analyzed. A continuous phase CGH is defined, and conditions necessary for its realizability are derived. A discrete phase CGH is also defined, and the space–bandwidth product requirement of the computer-controlled recording device is determined.

Consider the optical system of Fig. 4 with an input light (real-valued) amplitude distribution $a_1(x,y)$ in the front focal plane P_1 of a lens L. A CGH is also located in plane P_1 and has amplitude transmittance $\exp[i\phi(x,y)]$, where $\phi(x,y)$ is the CGH phase. The output light (complex-valued) amplitude distribution $a_2(u,v)$ is in the back focal plane P_2 of lens L. The relationship between $a_1(x,y)$ and $a_2(u,v)$ is given approximately by the Fourier transform:

$$a_2(u,v) = \frac{1}{i\lambda f}\int_{-\infty}^{\infty} a_1(x,y)\exp\left\{i\left[\phi(x,y) - \frac{2\pi}{\lambda f}(xu+yv)\right]\right\} \times dx\,dy, \tag{1}$$

where λ is the wavelength, and f is the focal length of lens L. Following Bryngdahl[1,2] in approximating this integral by the method of stationary phase, it can be shown that a point (x,y) in plane P_1 is approximately mapped to a point (u,v) in plane P_2, where

$$\begin{bmatrix} x \\ y \end{bmatrix} \rightarrow \begin{bmatrix} u \\ v \end{bmatrix} = \begin{bmatrix} \frac{\lambda f}{2\pi}\frac{\partial\phi(x,y)}{\partial x} \\ \frac{\lambda f}{2\pi}\frac{\partial\phi(x,y)}{\partial y} \end{bmatrix}. \tag{2}$$

A. Continuous Phase CGH

Equation (2) defines a mapping given the CGH phase $\phi(x,y)$. For most applications, a mapping

$$\begin{bmatrix} x \\ y \end{bmatrix} \rightarrow \begin{bmatrix} u \\ v \end{bmatrix} = \begin{bmatrix} g(x,y) \\ h(x,y) \end{bmatrix} \tag{3}$$

is given, and the problem is to solve

$$\frac{\lambda f}{2\pi}\frac{\partial\phi}{\partial x} = g(x,y), \tag{4a}$$

$$\frac{\lambda f}{2\pi}\frac{\partial\phi}{\partial y} = h(x,y) \tag{4b}$$

for $\phi(x,y)$. If $g(x,y)$ and $h(x,y)$ have continuous partial derivatives in a simply connected region R in plane P_1, Eq. (4) has a solution if and only if[8,9]

$$\frac{\partial g}{\partial y} = \frac{\partial h}{\partial x}. \tag{5}$$

This implies via Eq. (4) that

$$\frac{\partial}{\partial y}\left(\frac{\partial \phi}{\partial x}\right) = \frac{\partial}{\partial x}\left(\frac{\partial \phi}{\partial y}\right), \tag{6}$$

which is intuitively appealing.

A large class of functions can be easily defined which satisfy Eq. (5). Using complex variables, let $z = x + iy$ and $z^* = x - iy$. If a complex function $f(z)$ is analytic, the functions $g(x,y)$ and $h(x,y)$ defined by

$$f(z^*) = g(x,y) + ih(x,y) \tag{7}$$

satisfy Eq. (5). This theorem is easily proven by noting that

$$f(z) = g(x,-y) + ih(x,-y) \tag{8}$$

and using the Cauchy-Riemann conditions[10] to give

$$\frac{\partial g(x,-y)}{\partial y} = \frac{-\partial h(x,-y)}{\partial x}, \tag{9}$$

which is equivalent to Eq. (5).

Other classes of functions satisfying Eq. (5) also exist. It is very important to note, however, that the promising mathematical development of Eqs. (2)–(7) is valid only within the approximation of the method of stationary phase.

B. Discrete Phase CGH

If a mapping given by Eq. (3) is required but $g(x,y)$ and $h(x,y)$ do not satisfy Eq. (5), a continuous-phase CGH is not possible. One solution is to subdivide the CGH into subholograms.[3,11,12] For example, the total area might be divided into an $M \times N$ rectangular array of regions R_{mn}, each of size $\Delta x \times \Delta y$. Let the coordinates of the center of region R_{mn} be (x_m,y_n). Then define

$$\frac{\lambda f}{2\pi}\phi(x,y) = g(x_m,y_n)x + h(x_m,y_n)y \tag{10}$$

for $|x - x_m| \le \Delta x/2$ and $|y - y_n| \le \Delta y/2$.

Since

$$\frac{\lambda f}{2\pi}\frac{\partial \phi}{\partial x} = g(x_m,y_n), \tag{11a}$$

$$\frac{\lambda f}{2\pi}\frac{\partial \phi}{\partial y} = h(x_m,y_n), \tag{11b}$$

this CGH will map all the points in region R_{mn} to a point-spread function centered at the point

$$(u_{mn},v_{mn}) = [g(x_m,y_n), h(x_m,y_n)]. \tag{12}$$

This is the desired geometric transformation in discrete form. Division into regions other than rectangles is possible. An example is given in Sec. IV.

The point-spread function in plane P_2 of each region is

$$W\left[\frac{(u-u_{mn})\Delta x}{\lambda f}, \frac{(v-v_{mn})\Delta y}{\lambda f}\right],$$

where $W(u,v)$ is the Fourier transform of the envelope of the amplitude transmittance of the region. For rectangular regions without weighting, the point-spread function is

$$\operatorname{sinc}\left[\frac{(u-u_{mn})\Delta x}{\lambda f}, \frac{(v-v_{mn})\Delta y}{\lambda f}\right].$$

In general, the point spread will have characteristic dimensions (defined by the half-intensity points)

$$p\frac{\lambda f}{\Delta x} \text{ by } q\frac{\lambda f}{\Delta y},$$

where p and q are of order unity.

If the transformed region in plane P_2 coinsists of an $M' \times N'$ rectangular array of point-spread functions, for the impulse responses of different CGH regions to be resolved, the transformed region must occupy an area of dimensions $M'p\lambda f/\Delta x \times N'q\lambda f/\Delta y$. Therefore, even without including a carrier frequency to prevent overlap between the zero and first diffracted orders, the CGH must contain spatial frequencies at least up to $M'p/2\Delta x$ and $N'q//2\Delta y$ in the x and y directions, respectively. The space–bandwidth product of a CGH which performs a geometric transformation of an $M \times N$ array to an $M' \times N'$ array is, therefore, $MM'p/2 \times NN'q/2$. For the simple case where $M = M' = N = N'$, the transformation of N^2 regions requires a CGH with a space–bandwidth product of order N^4 (see Ref. 13). This implies a severe limit on the number N achievable with existing recording devices.

IV. Experiment

One continuous and one discrete CGH were made using a rotating drum laser beam recorder. The CGH phases were encoded as the amplitude transmittance $t(x,y)$ of the hologram with

$$t(x,y) = k_1 + k_2\cos[\phi(x,y) + \alpha x + \beta y], \tag{13}$$

where k_1 and k_2 are constants, and α and β are spatial carrier frequencies. The CGH has a space–bandwidth product (SBWP) of 2048 × 2048 and 256 grey levels. The SBWP can be increased at the expense of greater computing time. The constants were approximately $k_1 = 0.5$ and $k_2 = 0.4$. Film nonlinearity was minimized by introducing a reciprocal nonlinearity in the digital data using calibration data and carefully controlling the film development process. The resulting absorption hologram is copied onto a dichromated gelatin plate to produce a high-efficiency phase hologram. This final hologram is termed a COHOE (computer originated holographic optical element).[14]

A. Discrete Phase CGH

The transformation chosen was

$$\begin{bmatrix} x \\ y \end{bmatrix} \rightarrow \begin{bmatrix} u \\ v \end{bmatrix} = \begin{bmatrix} \sqrt{x^2+y^2} \\ 0 \end{bmatrix}. \tag{14}$$

This corresponds to mapping rings in the x-y plane to points along the v axis in the uv plane. Applications for this CGH were described in Sec. II. Clearly, the transformation does not satisfy Eq. (5). The hologram was, therefore, divided into N concentric rings of average radius r_n and width Δr with

$$\phi(x,y) = 2\pi r_n x/\lambda f \tag{15}$$

for $|\sqrt{x^2+y^2} - r_n| \le \Delta r/2$.

Figure 5(a) shows a portion of the discrete CGH. Phase discontinuities can be seen at the ring boundaries.

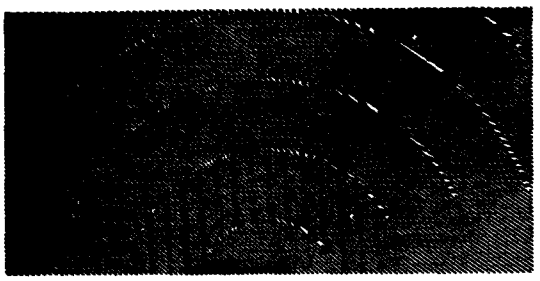

(a) Portion of CGH.

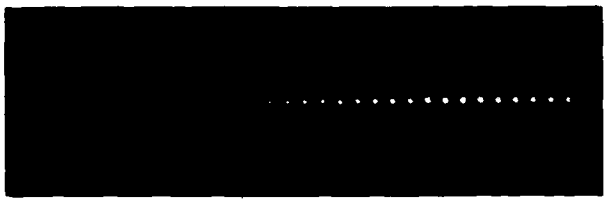

(b) All output points.

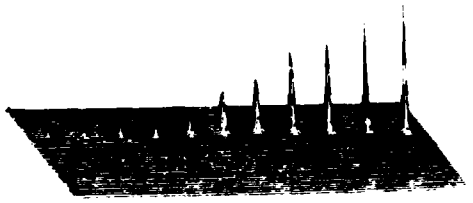

(c) First 11 points.

Fig. 5. Ring-to-point transform using discrete phase CGH: (a) portion of CGH; (b) all output points; (c) first eleven points.

(The grey scale of the fringes is not observable because of the high-contrast recording used in the reproduction process.) Figures 5(b) and (c) show the transformed output light distribution for a uniform input and $N = 30$. Figure 5(b) is a photograph of the thirty output points. The variation in output point intensities is due to the different areas of the rings. The significant sidelobe structures are essentially the impulse responses of ring-shaped apertures of varying radii. Figure 5(c) is an isometric plot of the points corresponding to the innermost eleven rings. For uniform illumination, the peak amplitudes of the output points are proportional to the areas of the corresponding rings. The ring areas range from $\pi(\Delta r)^2$ to $(2N-1)\pi(\Delta r)^2$. The dynamic range of the peak intensity of the output points is, therefore, $\sim 4N^2$. [Thus the number of points that could be accurately represented in Fig. 5(c) was limited by the TV camera used to acquire the data.] In most applications, the input light intensity will decrease with increasing radius, so the dynamic range of the output will not be extreme.

B. Continuous Phase CGH

Transformations which do not satisfy Eq. (5) are not realizable with the optical system of Fig. 4, which uses a single holographic element. However, some of these transformations may be implemented with optical

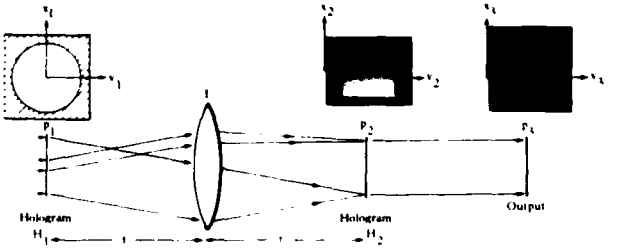

Fig. 6. Two hologram system for geometric transformation.

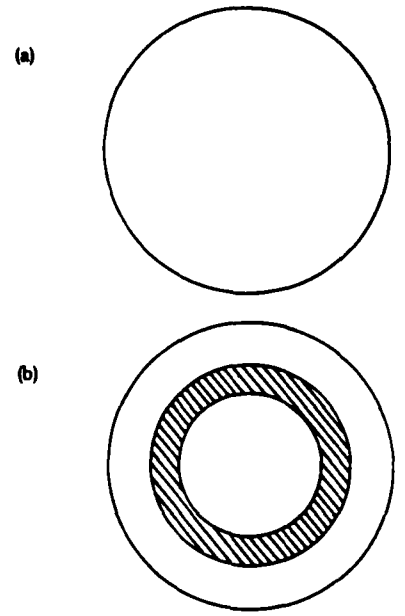

Fig. 7. Input light distributions: (a) uniform circular input; (b) input with opaque ring.

systems employing two or more holograms. A possible two-hologram system is given in Fig. 6. As for the system of Fig. 4, a CGH H_1 in plane P_1 and a Fourier transform lens L produce a transformed output in plane P_2. A second hologram H_2 (which may be computer-generated) in plane P_2 produces a second transformation in plane P_3. A lens can be used to Fourier transform or image between planes P_2 and P_3 if desired.

A circle-to-point transform may be accomplished with this system as follows: for CGH H_1, choose $f(z) = x_0 \ln z$, where x_0 is a real constant with units of length. The mapping is

$$\begin{bmatrix} x_1 \\ y_1 \end{bmatrix} \rightarrow \begin{bmatrix} x_2 \\ y_2 \end{bmatrix} = \begin{bmatrix} x_0 \ln(x_1^2 + y_1^2)^{1/2} \\ -x_0 \tan^{-1}(y_1/x_1) \end{bmatrix}. \tag{16}$$

and Eq. (5) is satisfied. Solving Eq. (4) gives

$$\phi(x_1,y_1) = \frac{2\pi x_0}{\lambda f}\left[x_1 \ln(x_1^2 + y_1^2)^{1/2} - y_1 \tan^{-1}(y_1/x_1) - x_1\right]. \tag{17}$$

This continuous phase CGH will map circles of radius r in the x_1y_1 plane to lines $x_2 = x_0 \ln r$ in the x_2y_2 plane. It should be noted that CGH H_1 is useful for scale and rotation invariant pattern recognition.[15,16] However, this application will not be considered here. The second hologram H_2 will transform lines x_2 = constant to

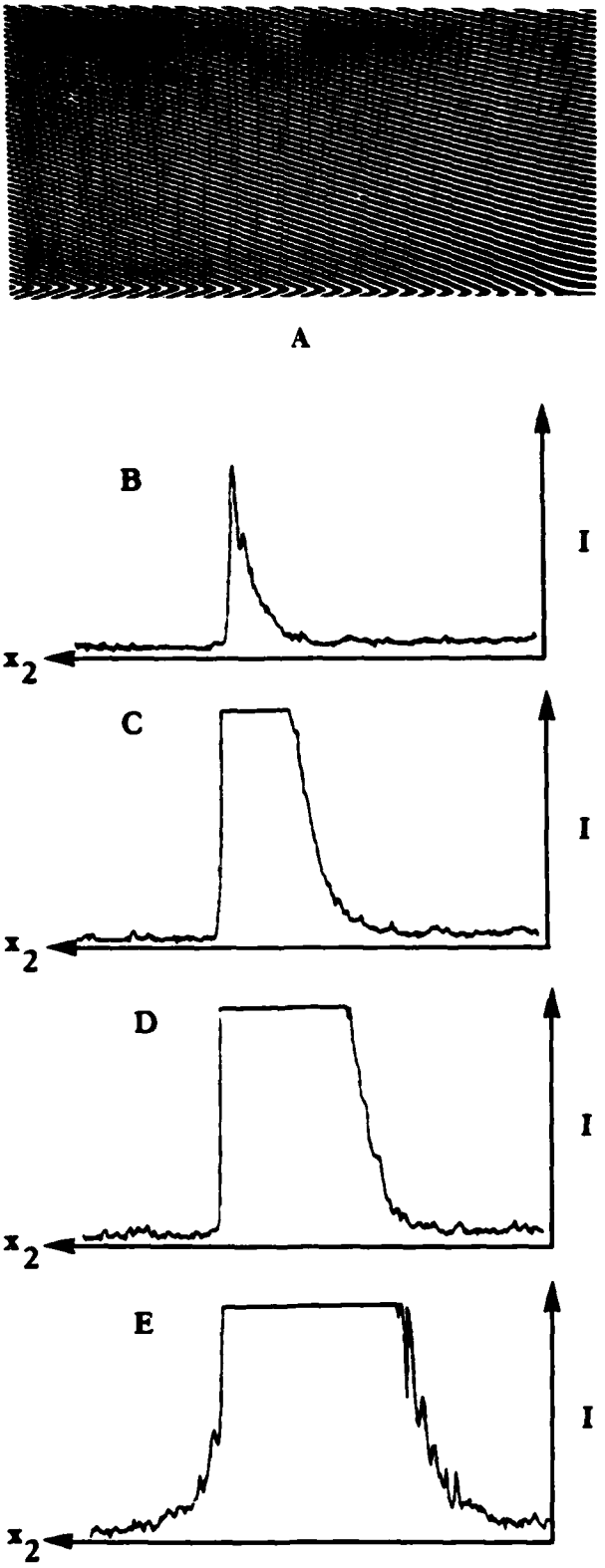

Fig. 8. Ring-to-line transform using continuous phase CGH: (a) Portion of CGH; (b)–(e) output intensity profiles for different input light levels for input of Fig. 7(a); (f) intensity profile for input of Fig. 7(b).

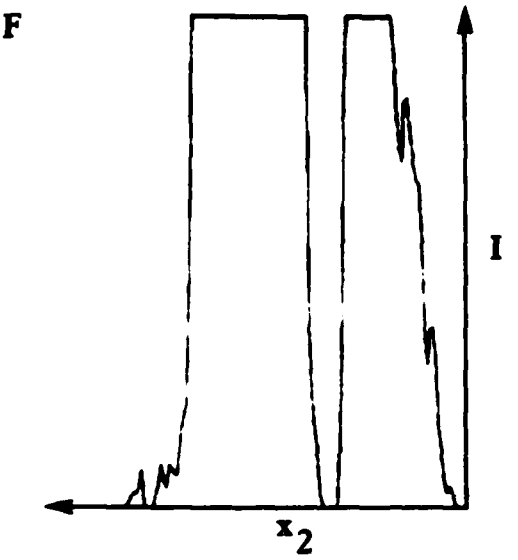

points in plane P_3. It can be interferometrically recorded using the wave front produced by uniform illumination of H_1 and a wave front diverging from a line focus at plane P_3. The resulting system requires one more component—the hologram H_2—than the ring-to-point system of Sec. IV.B but uses continuous phase CGHs and, therefore, should be capable of transforming inputs with much higher space–bandwidth product.

CGH H_1 was fabricated and tested using the input light distributions of Fig. 7. A portion of the continuous CGH is shown in Fig. 8(a). For the uniform circular input of Fig. 7(a), a photograph of the output light distribution in plane P_2 is inset in Fig. 6. Figures 8(b)–(e) show the intensity profile along the x_2 axis. The input intensity was varied to show different intensity regions relative to TV camera saturation. For an input with an opaque ring [Fig. 7(b)], the output intensity profile is shown in Fig. 8(f). The intensity profile has a high dynamic range and saturates the TV camera, except at the location corresponding to the opaque ring in the input. The demonstrates that rings are indeed transformed to lines.

Hologram H_2 is a conventional hologram and was fabricated interferometrically. For the uniform input of Fig. 7(a), the output light distribution in plane P_3 is shown in Fig. 9(a) and an isometric plot in Fig. 9(b). For the input with an opaque ring [Fig. 7(b)], the output photograph and corresponding isometric plot are shown in Figs. 10(a) and (b). Clearly, the two hologram system collects light from an input ring to a single point with the location of the point determined by the radius of the ring. The continuous nature of this transform as shown in Fig. 9(a) can be compared with the discrete transform of Fig. 5(b).

V. Conclusion

To design a system which uses CGHs to perform a geometric transformation, the continuous-phase CGH should be considered first. Although only applicable to mappings satisfying Eq. (5), it has the advantage of

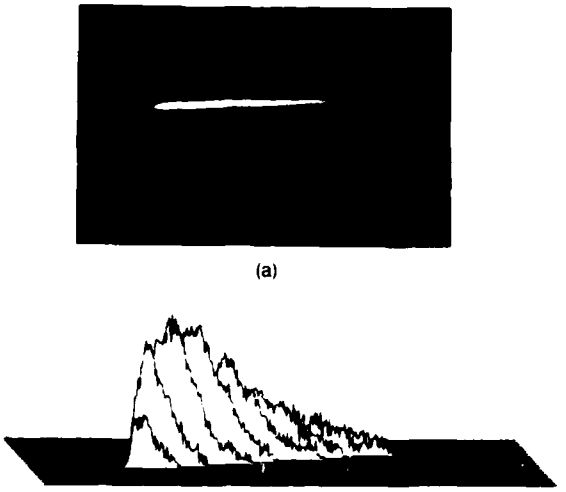

Fig. 9. Ring-to-point transform using two hologram system with uniform input [Fig. 7(a)]: (a) output photograph; (b) isometric plot.

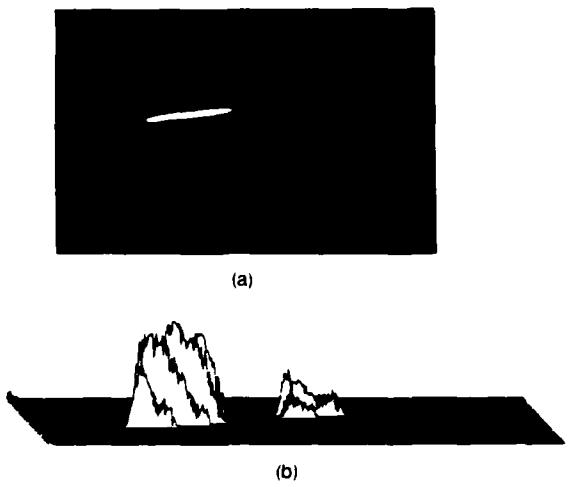

Fig. 10. Ring-to-point transform for input with opaque ring [Fig. 7(b)]: (a) output photograph; (b) isometric plot.

providing a high-resolution continuous transformation with no phase errors or discontinuities to cause incorrect phasing between adjacent points or undesirable sidelobes. This advantage is subject to the limits of the validity of the method of stationary phase. If the required transform does not satisfy the mathematical criterion, a system using multiple holograms should be considered. No design procedure has yet been established for this type of system, however. A discrete phase CGH is always possible. The disadvantage is that sidelobes of each point and interference between the sidelobes of adjacent points in the output plane as well as the requirement on the recording device of order N^4 points tend to limit useful resolution.

Both continuous and discrete CGHs for transforming rings to points have been fabricated and are suitable for applications in several areas including angle-wavelength multiplexing for optical fiber communication. Given the increased availability of large space–bandwidth recorders, significant work in CGHs for geometric transformations can be expected. In particular, the performance and flexibility of both one and two hologram systems deserve continued investigation.

This work was supported in part by the U.S. Army Research Office under contract DAAG29-81-K0129.

References

1. O. Bryngdahl, "Optical Map Transformations," Opt. Commun. **10**, 164 (1974).
2. O. Bryngdahl, "Geometrical Transformations in Optics," J. Opt. Soc. Am. **64**, 1092 (1974).
3. S. K. Case, P. R. Haugen, and O. J. Løkberg, "Multifacet Holographic Optical Elements for Wave Front Transformations," Appl. Opt. **20**, 2670 (1981).
4. G. Häusler and N. Streibl, "Optical Compensation of Geometrical Distortion by a Deformable Mirror," Opt. Commun. **42**, 381 (1982).
5. A. W. Lohmann and N. Streibl, "Map Transformations by Optical Anamorphic Processing," Appl. Opt. **22**, 780 (1983).
6. G. Herskowitz, H. Kobrinski, and U. Levy, "Angular Division Miltiplexing in Optical Fibers," Laser Focus **19**, 83 (Feb. 1983).
7. A. M. Tai and A. A. Friesem, "Transmission of Two-Dimensional Images Through a Single Optical Fiber by Wavelength-Time Encoding," Opt. Lett. **8**, 57 (1983).
8. W. S. Colburn and R. C. Fairchild, "Design Study for a Low-Distortion Holographic HUD," AFWAL-TR-81-1263, (1982), pp. 15–17.
9. W. Kaplan, *Advanced Calculus* (Addison-Wesley, Reading, Mass., 1959), pp. 244–249.
10. H. Hamilton, *Complex Variables* (Wadsworth, Belmont, Calif., 1966), pp. 28–39.
11. S. K. Case and P. R. Haugen, "Partitioned Holographic Optical Elements," Opt. Eng. **21**, 352 (1982).
12. H. Bartelt and S. K. Case, "Coordinate Transformations via Multifacet Holographic Optical Elements," Opt. Eng. **22**, 497 (1983).
13. P. Chavel *et al.* in *Technical Digest, Tenth International Optical Computing Conference* (IEEE Computer Society and ICO, New York, 1983), pp. 6–12.
14. R. C. Fairchild and J. R. Fienup, "Computer-Originated Aspheric Holographic Optical Elements," Opt. Eng. **21**, 133 (1982).
15. Y. Saito *et al.*, "Scale and Rotation Invariant Real Time Optical Correlator Using Computer Generated Hologram," Opt. Commun. **47**, 8 (1983).
16. C. L. Giles and H. H. Szu, "Optical Implementation of Coordinate Transformations for Pattern Recognition," J. Opt. Soc. Am. **73**, 1860 (1983).

END

FILMED

3-86

DTIC